AD-A190 223 REAL-TIME STRESSED CHANNEL SIMULATOR(U) TCS INC SAN DIEGO CA 10 DEC 87 TCS-TP-87-059 N00014-87-C-0133 1/1

UNCLASSIFIED F/G 15/3.1 NL

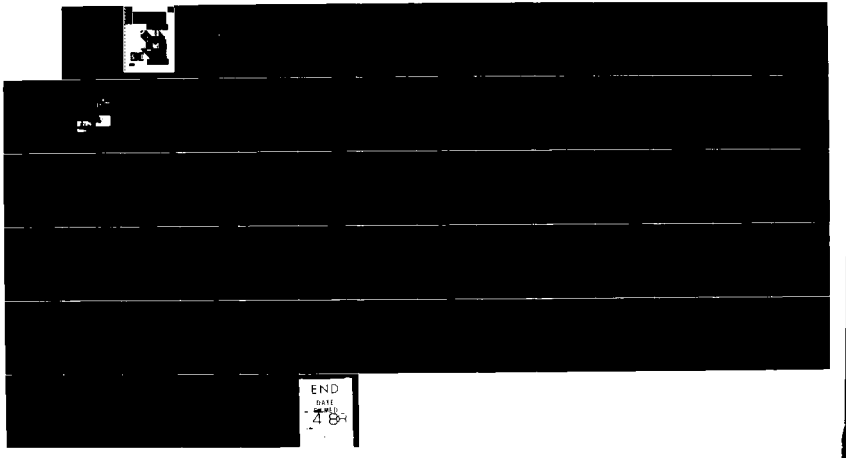

END
DATE
FILMED
4-88

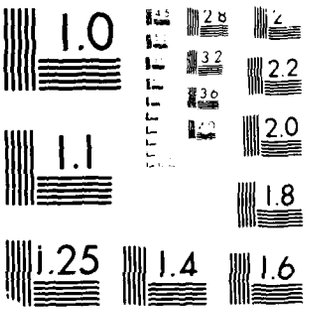

TCS-TP-87-059

(2)

REAL-TIME STRESSED CHANNEL SIMULATOR
FINAL REPORT

Contract N00014-87-C-0133

10 December 1987

Prepared for:

Office of Naval Research
Department of the Navy
800 N. Quincy Street
Arlington, Virginia 22217-5000

Prepared by:

TCS, Inc.
2560 1st Avenue
Suite 105
San Diego, CA 92103

Richard W. Middleton 12/8/87
Author Date

E. C. 12/8/87
Manager Date

EXECUTIVE SUMMARY

The Strategic Defense Initiative (SDI) research efforts are directed at a number of system architecture options involving space, airborne, and terrestrial platforms. A major consideration in the system architecture is the resolution of the battle management (BM) concept. To resolve the many complex issues, the Strategic Defense Initiative Organization (SDIO) has recognized the need for a real-time test facility. A common requirement in all of the architectures is the need for communication, command, and control (C^3) data links between the various platforms. The link or communication channel conditions are relatively benign during peacetime; however, in wartime situations, during pre-, trans-, and post-attack periods, the channel conditions degrade rapidly causing severe disruptions in C^3. The approaches to battle management, as they are tailored to the various architecture options being considered, will depend heavily upon the communication link integrity. This research is significant and timely in that it relates to the National Test Bed (NTB), in support of the SDI full-state development decision process. The NTB program is presently being undertaken by major contractors and involves the design, development, and installation of both experimental and simulation capabilities at the National Test Facility (NTF) and at remote facilities to form the NTB.

This Phase I research effort takes a major step in configuring a Real-Time Stressed Channel Simulator (RTSCS) to evaluate BM/C^3 concepts for the SDI program. The RTSCS consists of a personal computer (PC) and a hardware channel simulator. The PC computes the disturbed channel parameters, from operator specified conditions, and controls the hardware simulator, which in turn disturbs the signals under test as they would be in a real nuclear disturbed environment. The channel parameters are updated by the PC as the real-time dynamics of the link evolve. Radio frequency systems operating from ultra-high-frequency (UHF) to extremely-high-frequency (EHF) are accommodated by both the PC computational algorithms and the hardware equipment. An alternate configuration of the RTSCS consists of the PC and a host computer. In this configuration, the PC computes the channel characteristics

for the software simulation of equipment and network concepts by the host computer. Although much of the discussion in this report is centered around communication links and networks for C^3 application, the RTSCS can also be used to evaluate radar and active sensor waveforms in a stressed environment.

The two principal objectives of this research effort have been successfully completed. First, the software code, enabling the PC to evaluate the necessary channel parameters between arbitrarily specified platforms under a variety of nuclear scenarios, was completed. Secondly, several hardware channel simulators were identified and considered in terms of the PC interface requirements. The hardware simulators are: the Advanced Channel Simulator (ACS) built by MAXIM Technologies, Inc. and the Nuclear Effects Link Simulator (NELS II) built by the General Electric Co. Both of these simulators were developed through sponsorship by the Defense Nuclear Agency (DNA).

In applying the results of this research, whether it be for the purpose of experimentation or simulation, the operator must specify (for example) a satellite constellation, together with airborne and terrestrial platforms as may be required. A communication path, consisting of communication links between satellites (crosslinks) or between satellites and airborne or terrestrial platforms, is then identified. A nuclear scenario, based upon the geographic location and yield of a nuclear detonation, is then selected. The PC software program will evaluate the time evolution of the necessary communication link parameters for direct application to the test being performed. Typical parameters are: the absorption in dB, total-electron-content (TEC), the Rytov scintillation index ($\bar{\chi}^2$), and the decorrelation time (τ_0). The time evolution of the various link parameters involves the satellite(s) motion in the orbit(s), the terrestrial and airborne platform motion, the earth's rotation, and the expanding electron density contours as a function of the time-after-blast (TAB). The satellite orbit specification is very general and allows for elliptical, circular, polar, equatorial, or inclined orbits with arbitrary perigee altitudes. A major emphasis is

placed on the operator interface and the graphical display of the dynamics of the communication links with the passage of time. In this regard, the graphical display depicts the satellite motion around the earth, the nuclear disturbed region, and the selected link path(s).

The Phase I research effort discussed in this report provides an important first step in characterizing many of the concepts involving the RTSCS. In addition, a great deal of the computer code for the Stress Channel Computer (SCC) is complete. Throughout this research, dialogues with Department of Defense (DoD) agencies and contractors provided direction towards real applications. The Phase II research will complete these first steps and result in a fully operational RTSCS. The major areas of focus in the Phase II research are: 1) interface the SCC with a hardware channel simulator and demonstrate the disturbances to a test signal, 2) build or purchase a low cost flat fade (non-frequency selective) hardware simulator, 3) develop a user friendly data input capability for the SCC, 4) expand the capabilities of the real-time graphical display and include split screen depiction of scenario graphics and the graphing of selected channel parameters, 5) expand the nuclear scenario data base, and 6) refine and extend the signal processing functions within the SCC to include three-dimensional electron density data profiles. The refinements will include curve fitting in time and space to result in smooth transitions between and within the stored data files.

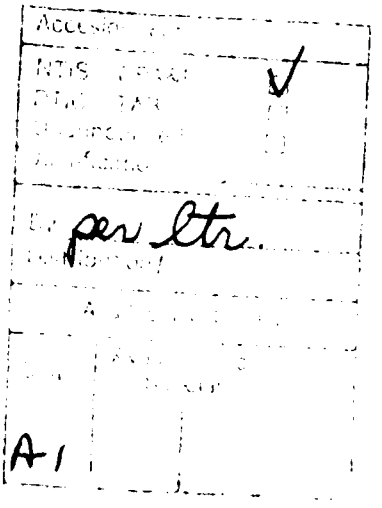

CONTENTS

1.0 INTRODUCTION

The Strategic Defense Initiative (SDI) research efforts are directed at a number of system architecture options involving space, airborne, and terrestrial platforms. A major consideration in the system architecture is the resolution of the battle management (BM) concept. To resolve the many complex issues, the Strategic Defense Initiative Organization (SDIO) has recognized the need for a real-time test facility. A common requirement in all of the architectures is the need for communication, command, and control (C^3) data links between the various platforms. The link or communication channel conditions are relatively benign during peacetime surveillance; however, in wartime situations during pre-, trans-, and post-attack periods, the channel conditions degrade rapidly causing severe disruptions in C^3. The approaches to battle management, as they are tailored to the various architecture options being considered, will depend heavily upon communications link integrity. For these reasons, the SDIO has sponsored this research to determine the technical merit and feasibility of a Real-Time Stressed Channel Simulator (RTSCS). To accomplish this task, two principal objectives were established. The first objective involves characterizing arbitrarily specified communication channels for nuclear scenarios aimed at disrupting strategic or tactical communications. The second objective involves identifying existing hardware channel simulators, which will use the resulting disturbed channel parameters for the purpose of evaluating signal and network performance in a battle management test facility.

This research characterizes the spatial and time evolution of a nuclear disturbed environment and evaluates the impact upon communication links involving satellite, airborne, and terrestrial platforms. The disturbances to the communication signal, often referred to as scintillation, result from high concentrations of electrons along the communication path. The electron distributions in space and time are quantified in terms of the location and yield of a nuclear detonation using elaborate computer codes. The resulting electron density profiles are then stored on standard 360K byte floppy disks for use by the RTSCS. The RTSCS consists of a personal computer (PC) and a hardware channel simulator. An alternate configuration consists of a PC and a host computer. The PC computes a variety of channel parameters from the

electron density data base and user specified link geometries. The channel parameters are then used to control the hardware channel simulator or, alternately, the host computer channel processing. The channel parameters are updated by the PC as the real-time dynamics of the link environment evolve. Radio frequency systems operating from ultra-high-frequency (UHF) to extremely-high-frequency (EHF) are evaluated by the RTSCS. This Phase I study has identified the Defense Nuclear Agency (DNA) Advanced Channel Simulator (ACS) and the Nuclear Effects Link Simulator (NELS-II) as existing hardware simulators. Both the ACS and the NELS-II are large hardware simulators which provide for frequency selective fading of the signal under test. Considerable economies can be realized in the hardware simulator by providing a flat (non frequency selective) fading characteristic which applies to a number of communication applications. In the remainder of this report, however, we shall refer to the channel simulator as the Advanced Channel Simulator or simply ACS. Throughout this report, the application of the RTSCS is focused on communication links and networks for C^3; however, the RTSCS is equally applicable to the test and evaluation of radar and active sensor signals. A functional description of the RTSCS, as it relates to the ACS, is shown in Figure 1.

Apart from using the ACS, the RTSCS can also be configured to interface directly or indirectly with large software network simulation programs. This configuration is referred to as the simulation test configuration. The functional description of the simulation test configuration with a direct interface to the host computer is shown in Figure 2. In the indirect interface configuration, the time history of the channel characteristics are computed off-line by the PC and placed on magnetic tape or diskettes, which are subsequently used by the host computer. The large programs of the host computer typically evaluate message throughput and reliability using multilayered protocols which connect many users through a variety of communication links employing different modulation wavefo.ms and operating frequencies. In this configuration, the performance results may not be processed in real-time, depending upon the speed and size of the host computer.

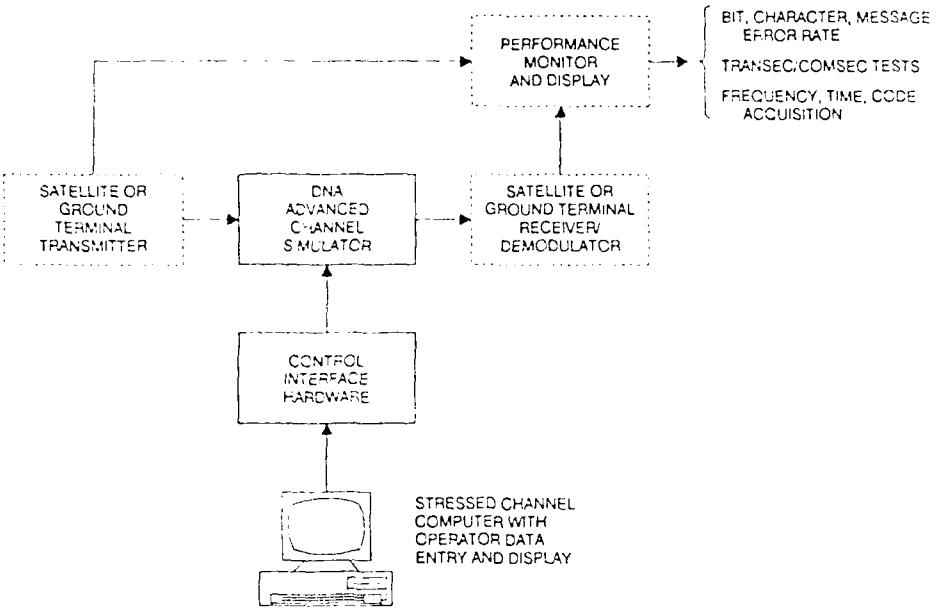

a) Laboratory Setup

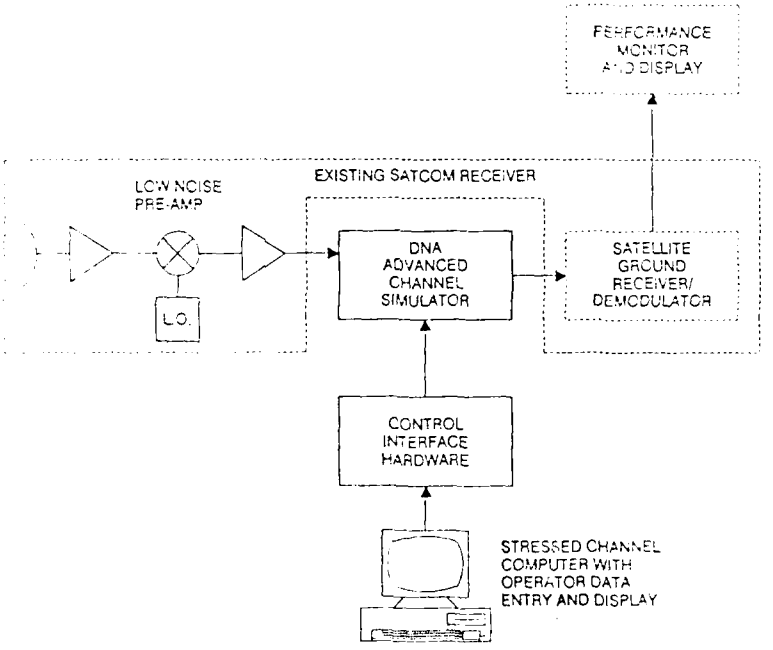

b) In-Circuit Setup

Figure 1. Functional Operation of the RTSCS (Solid Lines) in a BM/C^3 Experimental Test Configuration

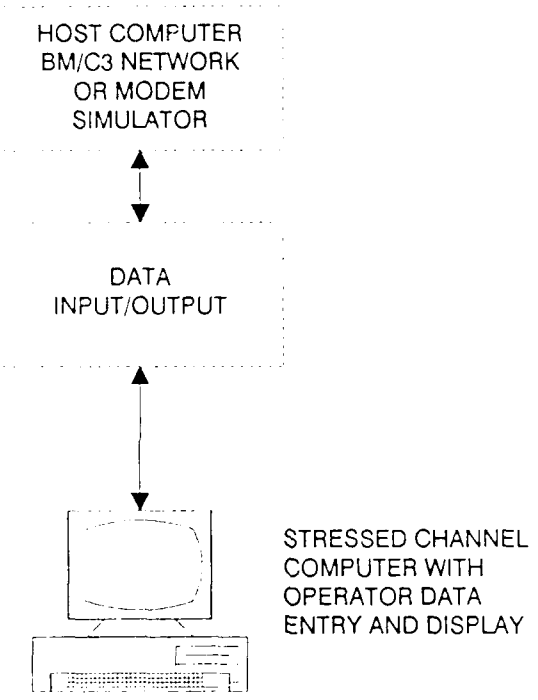

Figure 2. Functional Operation of the RTSCS (Solid Lines) in a BM/C^3 Simulation Test Configuration

This research is significant and timely in that it relates to the National Test Bed (NTB) program (Ref. 1) in support of the SDI full-scale development decision process. The NTB program is presently being undertaken by major contractors and involves the design, development, and installation of both experimental and simulation capabilities at the National Test Facility (NTF) and at remote facilities to form the NTB. Initially, dedicated service is planned to connect the NTF at Falcon Air Force Station (AFS), Colorado with: (1) the Strategic Defense Initiative Organization (SDIO), Washington, D.C., (2) the Army Strategic Defense Command (SDC), Huntsville, AL, (3) the Naval Research Laboratory (NRL), Washington, D.C., (4) the Dept. of Energy, Los Alamos National Laboratory (LANL), Los Alamos, NM, (5) the Air Force Electronic Systems Division (ESD), Hanscom AFB, MA, (6) the Air Force Rome Air Development Center (RADC), Rome, NY, and (7) the Air Force Space Division (SD), Los Angeles, CA. The purpose of the NTB is to provide a comprehensive capability to compare, evaluate, and test alternative system and battle management/command, control, communications (BM/C^3) architectures for defense against ballistic missiles, as well as to evaluate various defensive technologies in a system framework. The RTSCS will provide a major data base for assessing the BM/C^3 in either natural or stressed channel environments.

The remainder of this report is organized as follows: In Section 2.0, the RTSCS is discussed from an operational point of view. Both the experimental test facility (Figure 1) and the simulation test facility (Figure 2) configurations are included in this discussion. The interface requirements and the preliminary design of the interface for the DNA-ACS are also reviewed in detail. Section 3.0 outlines the software code developed during this research to characterize the communication channel. The considerable amount of detail supporting Section 3.0 is relegated to Appendices A through C. Section 4.0 summarizes the results and conclusions.

2.0 Real-Time Stressed Channel Simulator (RTSCS): Configuration and Operation

The communication link design for the Space Defense Initiative (SDI) must maintain channel robustness during benign and/or wartime situations. It is therefore necessary to emulate natural and nuclear disturbances and study their effects upon various communication links under consideration. Figure 3 depicts a typical satellite communication network showing the regions in which the channels are disturbed. In effect, the RTSCS will provide a means for evaluating the communication network performance by modeling the channel disturbances within the framework of the various government test facilities (e.g., the National Test Bed).

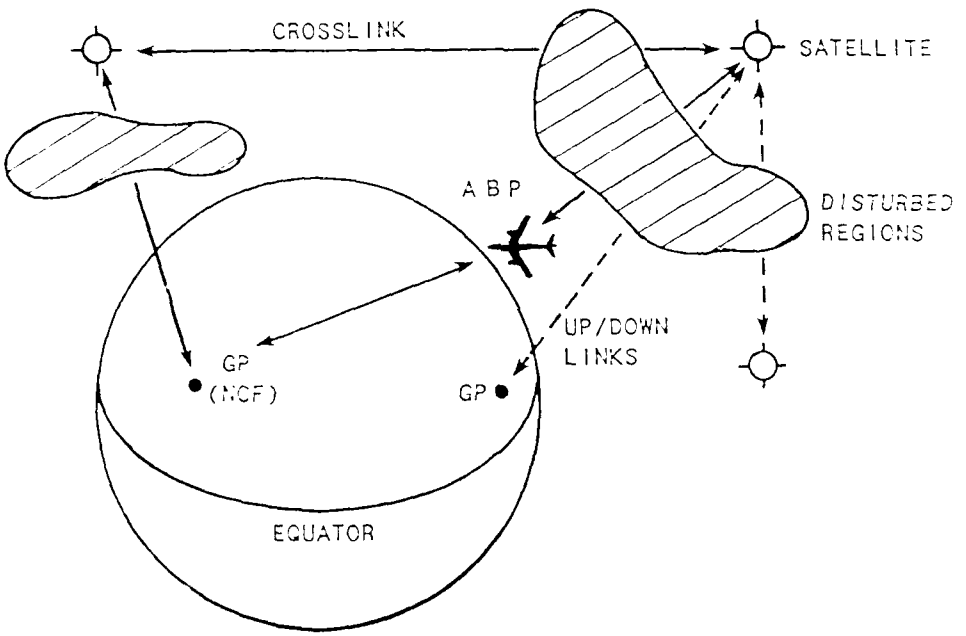

G.P. = Ground Platform
A.B.P. = Airborne Platform

Figure 3. Satellite Communication Links

The RTSCS emulates a variety of signal disturbances encountered along real communication paths. The propagation disturbances are classified as those resulting from an increase in the mean electron content and those resulting from spatial variations in the electron content which give rise to a non-homogeneous or striated propagation media. These generally give rise to static and dynamic signal disturbances. Examples of static signal disturbances are: absorption, noise, phase and doppler shift, time delay, and dispersion. Dynamic disturbances include: amplitude and phase scintillation, angular scattering, and time delay jitter. The stressed channel simulator will have, in memory or on floppy disks, the spatial and temporal electron density profiles for various detonation scenarios. The computer controlled simulator uses the operator selected communication path and electron profile geometries to compute the appropriate parameters which control the hardware (or software) elements of the channel simulators. This allows the operator to enter a nuclear scenario by the detonation yield and location and thereby examine the robustness of various communication links and their impact on battle management concepts. Figure 4 represents a collage of photographs of the existing hardware, which, when integrated together, form one of the RTSCS configurations. Referring to Figure 4, the Stressed Channel Computer (SCC) generates the channel parameters necessary to evaluate the system under test. The computational algorithms and parameters are discussed in detail in Section 3.0.

In setting up a test, the operator first selects a nuclear scenario. The electron density profiles for the scenario are loaded from a floppy disk. Typically, each scenario consists of five or six sets of electron density contours covering a period of time up to two or three hours after a blast. Following the scenario selection, the data necessary to completely define the communication links must be entered. The necessary parameters, with a brief description, are tabulated in Table I.

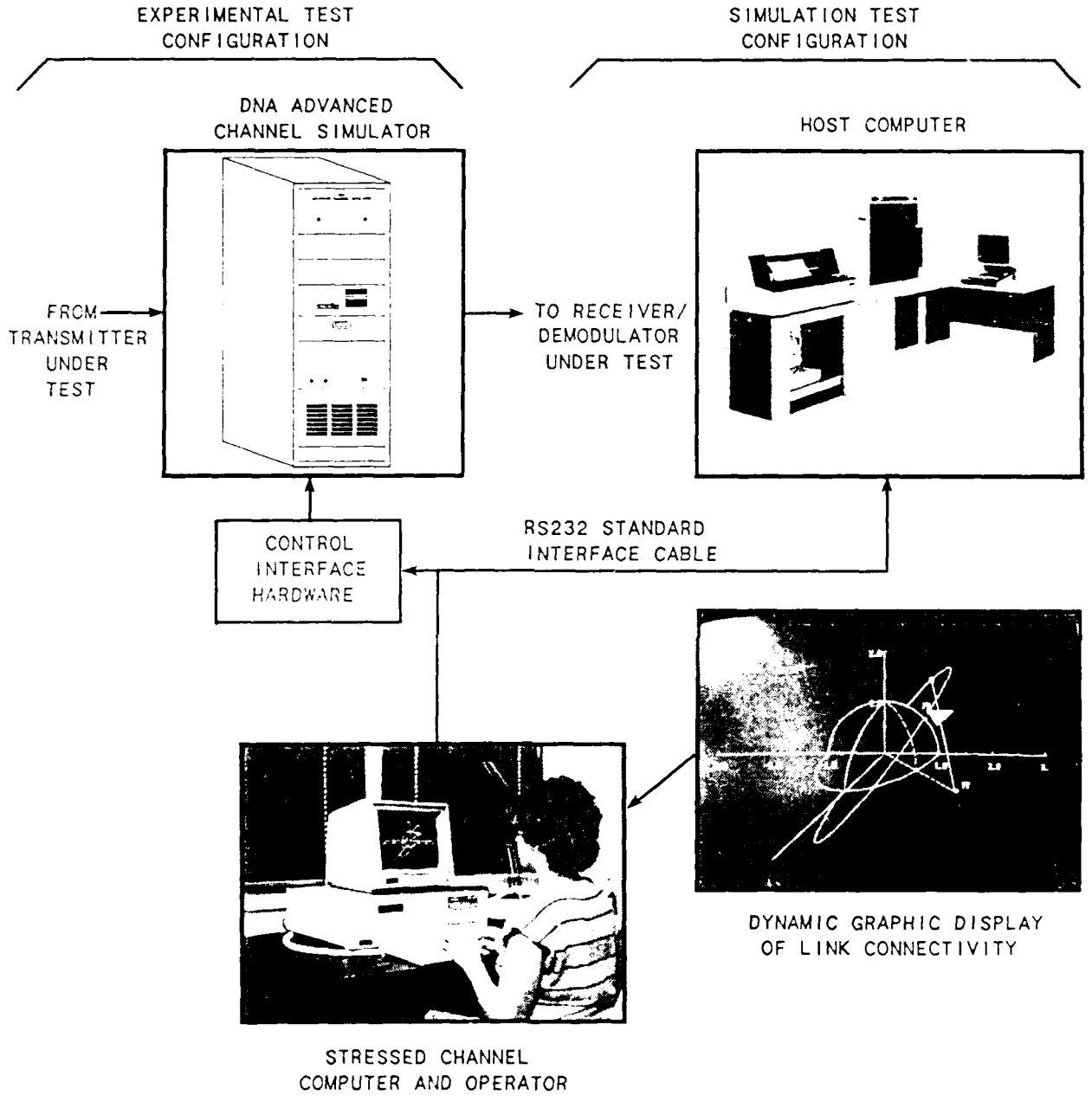

Figure 4. Depiction of Existing Equipment for the RTSCS Showing Alternate Configurations

Table I. Data Entry Parameters

Function	Description	Designation	Unit	Comment
Satellite orbit orientation	right ascension of ascending node	Ω	degree	Relative to vernal equinox at reference meridian.
	inclination	i	degree	0° = equatorial orbit 90° = polar
Satellite orbit orientation (continued)	longitude of perigee	ω	degree	
	Normalized Greenwich Mean Time	N.G.M.T.	-	At reference meridian normalized to t_p = 24 hrs.
Orbit shape	eccentricity	e	-	$0 \geq e \geq 1$ 0 = circular orbit
	Altitude at perigee	ALT	Km	
Satellite position in orbit	Time of perigee passage	τ_n	-	Normalized to orbital period T.
Satellites	Number of satellites per orbit	NSAT	Satellite	Satellites are equally spaced in iongitude.
Orbits	Number of orbits per constellation	NOBT	Orbits	Identical orbits equally spaced in longitude.
Blast point	Magnetic longitude	BLNG	degrees	
Receive/ Transmit Terminal	Latitude	TLAT	degrees	For fixed terrestrial terminal.
	Longitude	TLNG	degrees	
	Altitude	TALT	Km	

Table I. Data Entry Parameters (cont'd)

Function	Description	Designation	Unit	Comment
Transmit/ Receive Reference	Reference Satellite	NRS	-	For orbiting satellite reference.
	Reference Orbit	NRO	-	

By selecting Ω and the Normalized Greenwich Mean Time (N.G.M.T.) relative to a reference meridian, the satellite position above a rotating earth is established in an absolute sense. The reference meridian can be chosen to pass through a prominent location like Washington, D.C.; the blast point or a fixed terrestrial terminal meridian may also be chosen for determining the reference meridians. The blast point altitude and magnetic latitude influence the electron density contours and therefore are implicit in the scenario selection. By identifying the "receive/transmit terminal" and the "transmit/receive reference", the operator identifies a particular communication link along which the propagation disturbances will be computed. Although the entries in Table I suggest a link between a terrestrial terminal and a satellite, any combination of communications platforms can be selected. For example, if the "receive/transmit terminal" were identified as another satellite, the communication link would represent a satellite crosslink. In addition to characterizing a single link, the operator can also select a number of links to configure a communication network.

When the scenario and other test conditions have been entered into the SCC, the operator simply executes the program to begin the test. The SCC computes the parameters describing the disturbed channel for the specified link (or links) and outputs the parameters through an RS232 interface to either the ACS or the host computer, depending upon the test configuration. When configured with the ACS, the parameters are updated in real-time using the SCC internal real-time clock. Two major temporal events determine the parameter updating. The first event is the changing communication link geometry relative to the disturbed region. This is caused by the satellite and terminal motion along their trajectories and may require updating every

several seconds. The second event is the changing size of the disturbed region caused initially by the forces of the blast and, in latter times, by natural drift and recombinations of electrons. The updating for the disturbed region is dependent upon the selected scenario. Shortly after the detonation, the updating may be required every several minutes, diminishing to half-hour intervals at latter times. When interfacing with the host computer as in the simulation test configuration, the update times can be appropriately normalized to accommodate non-real-time performance evaluations.

A very useful capability provided by the SCC during the execution of the the test is the computer generated graphical display of events and parameter values as the test progresses. An example of this capability is shown in Figure 4 by the photograph of the operator's screen. In this photograph, the display shows the link between the satellite and a ground terminal at a point in time. The shaded area represents the disturbed region of the channel and the elliptical satellite orbit path is seen to be inclined relative to the geocentric coordinate axes. The graphical display provides system engineers with a means, to rapidly assess the test results as they relate to the disturbed channel.

The remainder of this section describes the two configurations of the RTSCS: (A) the Experimental Test Configuration using the ACS and (B) the Simulation Test Configuration using a host computer.

A. RTSCS - Experimental Test Configuration

The Experimental Test Configuration is intended for scientific or developmental engineering tests of hardware or software for the purpose of demonstrations or evaluating performance capabilities. Individual experiments may focus on one or more elements of the strategic defense system, ranging from the component level to integrated systems. The elements being tested may be brassboards, mockups, or development models. In this configuration, the RTSCS will interface with the radio frequency (RF) or intermediate frequency (IF) of the elements being tested. The communication or radar equipment may or may not be the principal subject of the test. For

example, if several RTSCS are configured as a network involving sensors, radars, and C^3, the experimental test can evaluate BM software concepts, including network control software. As noted in Figure 1b, the input may in fact be the downlink of an orbiting satellite. In any event, the principal function of the RTSCS is to evaluate the impact of the disturbed channel on the equipment or software being tested.

In the Experimental Test Configuration, the RTSCS consists of off-the-shelf equipment and customized software design packages. A full complement of equipment consists of:

1. Stress Channel Computer (SCC)
2. Defense Nuclear Agency (DNA)
   Advanced Channel Simulator (ACS)
3. RS232 interface cable
4. RF Mixers
5. Data Modem
6. Data Control Multiplexers

The last three items are required under special circumstances. The RF Mixers are required when the input and output RF test signals are not in the range of the ACS. The Data Modem is a standard 1200 or 2400 bps modem and is required when the SCC is remote from the ACS, as might be the case in the experimental test of a BM network. The Data Control Multiplexer is required when the SCC is to control more than one ACS, as would be required in a network evaluation. The SCC is a PC with a standard PC communication protocol package. The customized software for the SCC is the principal focus of this study. The RS232 interface cable is a standard 25 pin cable and provides a direct interface between the PC and the ACS.

The ACS is designed to emulate the fade characteristics of a typical Satellite Communication (SATCOM) channel caused by natural multipath effects or nuclear propagation disturbances. The ACS is a programmable channel simulator and provides a real-time modeling capability for nuclear and

ionospheric link effects. Figure 5 shows a block diagram of the ACS. The modeling effects include:

1. Signal absorption and blackout
2. Time delay and doppler
3. Dispersion
4. Flat and frequency selective fading (multipath)

The ACS has a simulation bandwidth of 76 MHz and a tuneable center frequency covering the range from 70 MHz to 8.5 GHz. Therefore, it can interface directly with the incoming RF signal or with the IF downconverter. The ACS fade parameters can be directly controlled by the ACS keypad, floppy disk, or remotely programmed via the RS232 interface. The programmable channel fade parameters include:

1. Decorrelation time - τ_0
2. Decorrelation frequency - f_0
3. Time history - N_1
4. Rayleigh frequency - f_r
5. Signal attenuation - K_A (for blackout simulation)
6. Noise Degradation - Additive-White-Gaussian-Noise (AWGN)

The ACS typically interfaces with the IF downconverter of the receiving RF antenna, but it can also interface directly with the incoming RF signal. As long as the signal is within the adjustable frequency range of the ACS, no other external equipment is required. The user can remotely program the ACS for the incoming signal frequency. If the incoming signal is outside the range of the ACS, a mixer with appropriate filtering can be inserted between the ACS and the receiver to shift the signal within the frequency range of ACS. The nominal input power level is -10 dBm; however, the range is adjustable from -50 to -10 dBm and can be placed under program control. Table II summarizes the characteristics of the ACS.

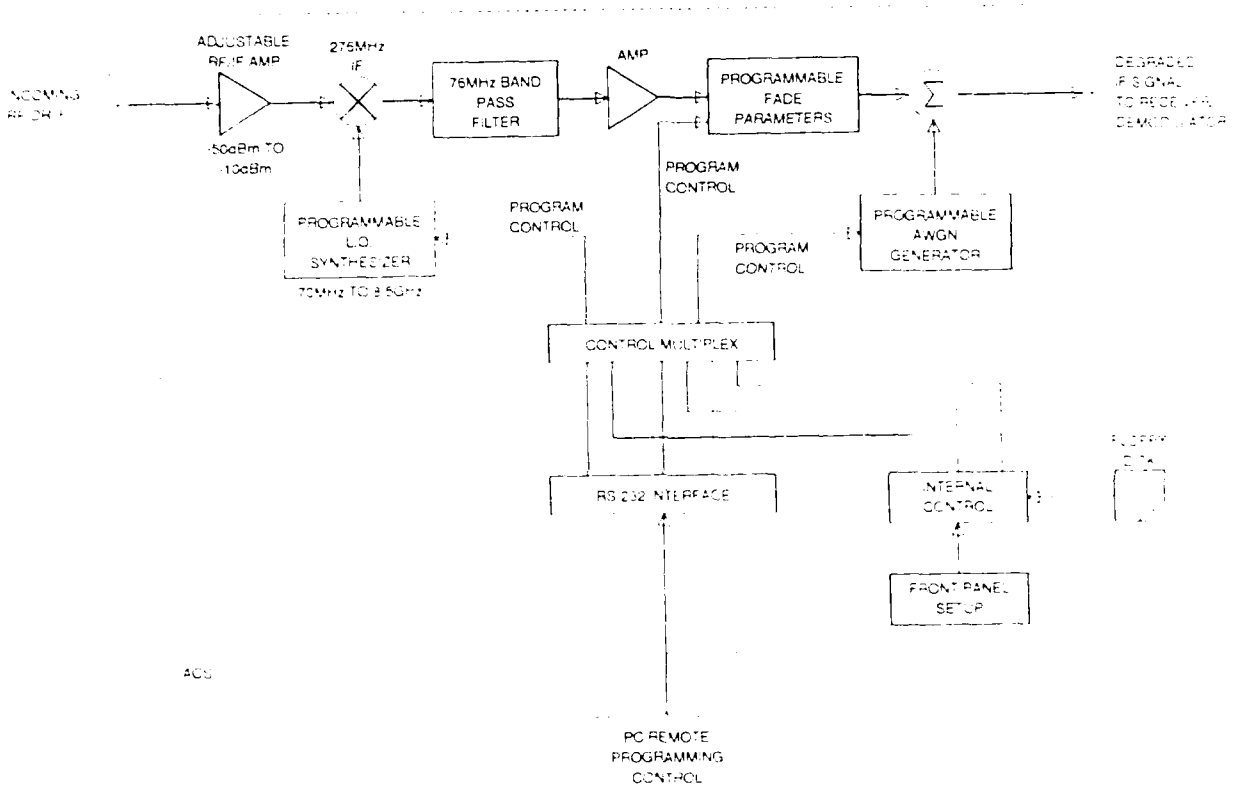

Figure 5. DNA Advanced Channel Simulator Block Diagram

Table II. ACS Characteristics

Parameter	Specification
Instantaneous Bandwidth	76 MHz
Decorrelation Time (τ_0)	1 msec to 100 sec
Decorrelation Frequency (f_0)	89 KHz min.
Update Interval	60 sec. min.
Fading Dynamic Range	+7 to -40 dB
Doppler and Rate	-20 to +20 KHz, 80 KHz/sec max
Delay and Rate	0 to 10 μsec, 20 μsec/sec max
Blackout Effects	
Attenuation Range	0 to 90 dB
Resolution	0.5 dB
Update Interval	0.5 sec.
AWGN Generator	
Output power	-135 dBm to 0 dBm
Stability	0.1 dB
Bandwidth	100 MHz
Noise Floor	-43 dBm
Programmable RF Converter	
Input Tuning Range	70 MHz to 8.5 GHz, 1 KHz steps
Bandwidth	70 MHz to 300 MHz, 40 MHz steps 300 MHz to 8.5 GHz, 100 MHz steps
Input level	-50 dBm to -10 dBm
Noise Figure	12 dB
AGC	Software controlled

B. RTSCS - Simulation Test Configuration

The Simulation Test Configuration is intended for the execution of one or more software programs for the purpose of predicting the performance of various components of a strategic defense system. Figure 2 depicts the RTSCS in the Simulation Test Configuration. The RTSCS interfaces directly with a host computer which uses the communication channel parameters to evaluate communication networks or equipment. In this configuration, the host computer contains the appropriate software to model the system functions being tested.

As an example application of the Simulation Test Configuration, suppose that a BM network concept is being evaluated and that the host computer contains a data base for the performance of a communication modulator/demodulator (modem). The modem is described in terms of the types of waveform modulation, error-detection-and-correction coding (EDAC), time and frequency diversity combining, data rate, etc. The performance of the modem, which forms the data base, is the bit, character, or message error probability, the acquisition time, etc. which are characterized in terms of the disturbed channel parameters. Examples of typical data bases are shown in Figures 6 and 7 for differentially-coherent binary phase-shift-keying (DC-BPSK) waveform modulation. In both figures, the amplitude variations caused by the channel disturbance correspond to the Rayleigh regime, for which $\bar{\chi}^2 > 0.1$. The results of Figure 6 correspond to a rate 1/2, constraint length 3 convolutional EDAC code, and $N_c = 2$ bit non-coherent combining. The performance will not continue to approach the ideal performance with decreasing τ_o/T_b, as shown in the figure. Instead, it will abruptly degrade for $\tau_o/T_b < 2$ because of the lack of phase coherence between adjacent bits. Figure 7 shows the improvements to be gained using a rate 1/2, constraint length 7 convolution EDAC code with several conditions of non-coherent bit combining (N_c). The data bases, represented by Figures 6 and 7, are simply representative of commonly used schemes to increase the throughput and reliability of communication links. Similar data bases must be developed for a variety of SDI links and stored at the various network nodes for evaluating the SDI network and link design concepts.

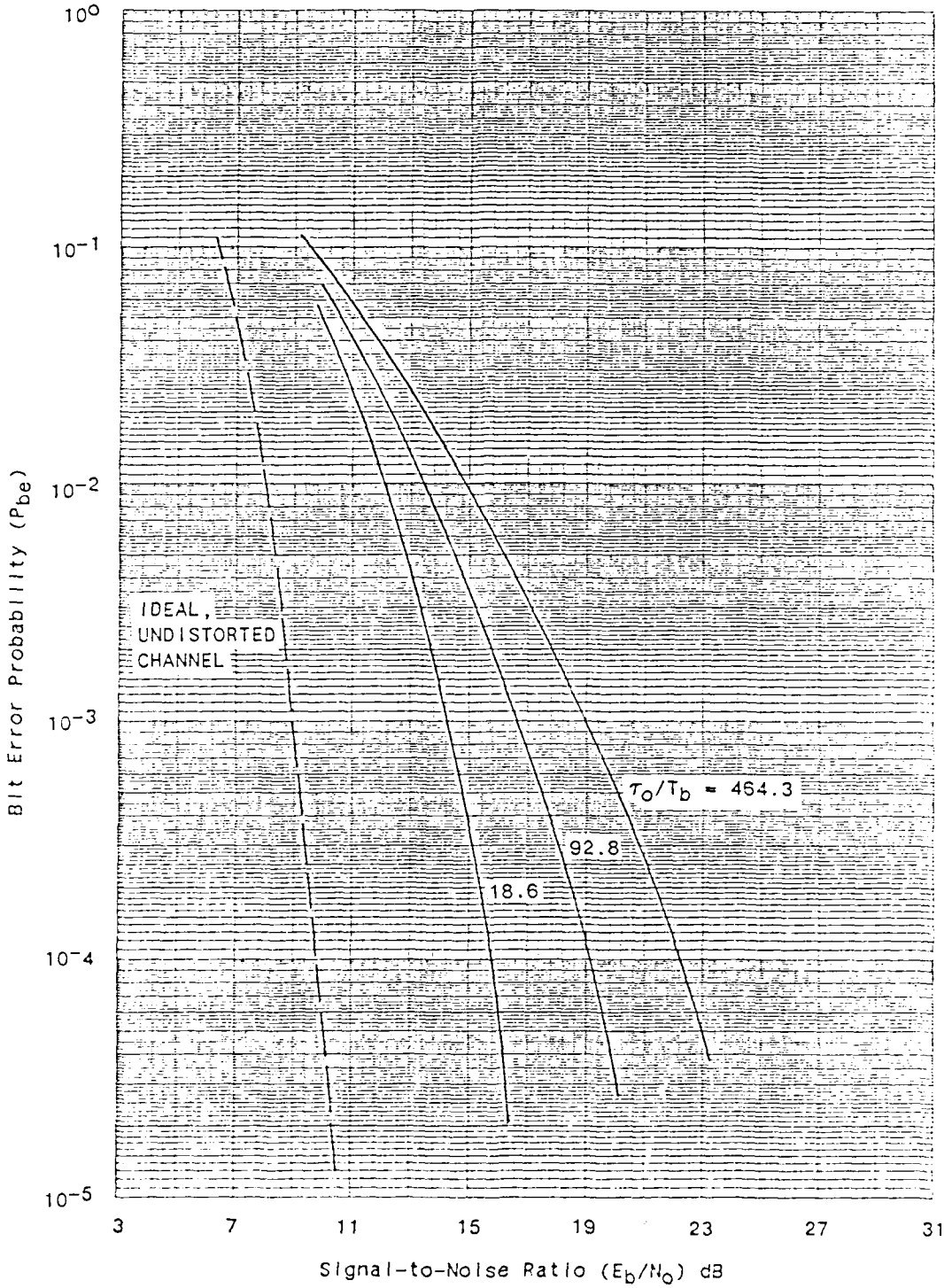

Figure 6. Performance of DC-BPSK for Several Values of τ_o/T_b with Non-coherent Combining (N_c=2) and R 1/2, K=3 Convolutional Coding

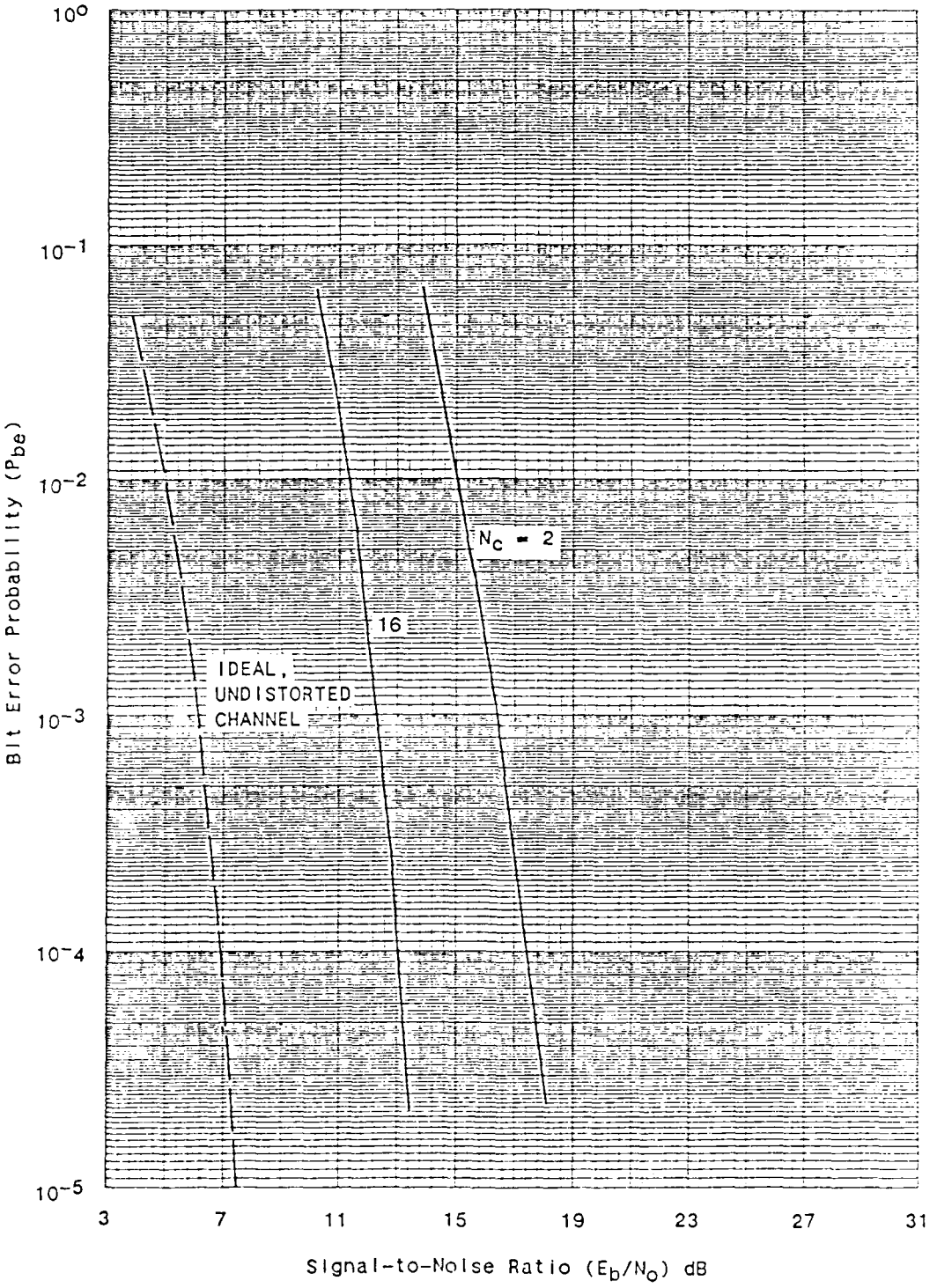

Figure 7. Performance of DC-BPSK in Slow Rayleigh Scintillation ($\tau_o >> T_b$) with Non-coherent Combining (N_c) and R 1/2, K=7 Convolutional Coding

With the performance data base for each link node stored in the host computer, the data flow throughout the network can be evaluated based upon the network protocol software instructions. For example, suppose that critical satellite sensor data is to be sent to an earth terminal for evaluation at the National Command Facility (NCF). The originating satellite may broadcast the data to a neighboring satellite on an EHF communication crosslink and to an airborne terminal via a UHF downlink. This situation is depicted by the heavy lines in Figure 3. If the crosslink uses DC-BPSK waveform modulation, the data base at the relay satellite will be as shown in Figures 6 or 7. Typically, a variety of downlink waveforms are available, so the airborne terminal and the NCF receiver terminals will utilize the appropriate communication link data base. As the sensor data arrives at the various nodes, after an appropriate delay, the probability of receiving the data without errors is computed for each individual node. From the results, the network simulator can then assess the probability of correctly receiving the sensor data and the resulting throughput delay. In this manner, the RTSCS will provide a valuable asset in evaluating various network concepts for the SDI program.

In the above examples, the communication data bases are assumed to be available. In fact, the Simulation Test Configuration of the RTSCS can also be used to establish the data bases. In this regard, the host computer software can simulate the modem functions and evaluate the error performance of the modem under a variety of channel conditions as provided by the SCC.

3.0 Stressed Channel Computer (SCC): Processing Overview

The purpose of the Stressed Channel Computer (SCC) is to compute the disturbed channel parameters and provide the results to either the ACS or the host computer, depending upon the configuration of the RTSCS. The disturbed channel is characterized by a concentration of electrons in the ionosphere. Although the electron concentrations occurring in the natural ionosphere can interrupt communications, the principal interest here is the affect of high-altitude, high-yield nuclear detonations, whose purpose is to disrupt critical communication during wartime conditions. Extensive research has been conducted to characterize a nuclear detonation and the resulting impact upon RF propagation. These research efforts, principally sponsored by the Defense Nuclear Agency (DNA) and the Air Force Weapons Laboratory (AFWL), have matured to the point of influencing systems designs and specifications. The results presented in this section utilize this body of experience to model the behavior of communication links operating from UHF through EHF.

The electron concentrations, following a nuclear detonation, are characterized by large computer codes developed largely under DNA sponsorship. Quantitatively, the disturbed environment is described by spatial and temporal electron density contours. Although the computer codes compute the electron densities in three-dimensional space, the data is stored in data files as arrays of two-dimensional profiles representing "cuts" in three-dimensional space, as shown in Figure 8. A major role of the SCC is to generate the three-dimensional contours from the two-dimensional data files and then project the contours onto an oblique two-dimension plane containing the propagation path. A unique, although frequently encountered, situation arises when the electron density profile data is available only as a single two-dimensional data file. In this situation, the SCC generates the three-dimensional contour by rotating the data through an elliptical path. In this research, the electron density profile data is characterized in the magnetic field plane along a specified magnetic meridian, although some flexibility is available in applying the data to any magnetic meridian.

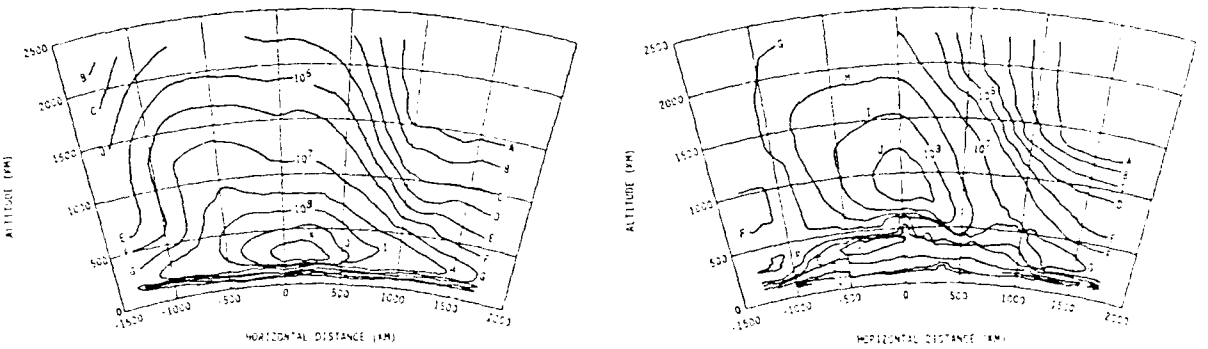

(a) (b)

Figure 8. Electron Density (Contours (CM^{-3}), (A=1x10^{-4}, B=3x10^{-4}, C=1x10^{5}, etc.). (a) TAB = 30 S., (b) TAB = 2 min.

The channel parameters, which characterize the communication link, are dependent upon the manner in which the propagation path intersects the three-dimensional electron density profiles. With regard to the media, the channel parameters are essentially dependent upon the total-electron-content (TEC) and the variation of the electrons along the propagation path, L_p. The relationships used in this section to describe the parameters are taken from reference 12. The TEC is denoted by N_T and is expressed as

$$N_T = \int_{\emptyset}^{L_p} n_e(z)dz \qquad \text{electrons/m}^2 \qquad (1)$$

where $n_e(z)$ is the electron density. The variation in the electron density is denoted by the variance $\sigma_e^2 = \overline{\Delta n_e^2}$. Because the small-scale electron density fluctuation, Δn_e, is not readily available, it is conservatively taken to result from 100 percent variations in the electron concentrations (i.e., $\Delta n_e = n_e$). The parameters required to control the ACS are listed in Table II and their functional dependence upon the media and communication link characteristics are,

$$\tau_o = 6.07 \times 10^{15} \frac{f_g}{\sqrt{L_p \sigma_e^2 \nu}} \quad \text{(seconds)} \tag{2}$$

$$f_o = 4.35 \times 10^{40} \left[\frac{L_x^2}{L_Z L_p^2}\right] \frac{f_g^4}{\sigma_e^2} \quad \text{(Hz)} \tag{3}$$

$$f_r = \left[2.6 \max \left(\overline{\chi^2}, .1\right) \tau_o\right]^{-1} \quad \text{(Hz)} \tag{4}$$

$$K_A = 1.16 \times 10^{-19} \frac{N_T}{f_g^2} \quad \text{(dB/m)} \tag{5}$$

where

$$\overline{\chi^2} \simeq 1.138 \times 10^{-32} \frac{L_Z L_p^2}{L_X^2} \left[\frac{\sigma_e^2}{f_g^3}\right] \tag{6}$$

The constant ν in equation (2) is the relative velocity (in meters/sec) of the communication platforms and the media drift in the plane of the receiving antenna. The parameter f_g is the operating frequency of the communication platforms expressed in GHz and the formulas generally apply from $0.3 \leq f_g \leq 300$ (i.e., from UHF through EHF). The parameters L_x, L_y, L_z are propagation path-aligned scale sizes of the structured media and are related to the magnetic field aligned scale sizes L_r, L_s, L_t, having typical values 10, 1, and 1 Km respectively. These parameters form orthogonal coordinate systems in which L_z is aligned with the propagation path and L_t is aligned with the magnetic field line. A conservative characterization of the channel results when $L_x=t_r$, $L_y=L_s$, and $L_z=L_t$ under all geometric conditions.

The geometry of a typical situation is shown in Figure 9, in the framework of the geocentric magnetic coordinates X_m, Y_m, Z_m. The magnetic coordinates are used as the reference simply because the electron density contour data is stored relative to the earth's magnetic field. The electron density contours are characterized by plumes which extend into the magnetosphere. These plumes generally follow the earth's magnetic field lines and thus bend toward the magnetic equator, as shown in Figure 9. The point B denotes the point on the earth's surface directly under the blast point and the points S and T denote the satellite and terminal points, respectively. The satellite is shown to be in an orbit inclined with parameters (Ω',i', ω') which are the magnetic coordinate counterparts of (Ω, i, ω), defining the orbit in geographic coordinates. Appendix A discusses the details of the transformations between coordinates and Appendix B discusses the satellite orbits and their specification. The Magnetic Field Plane (MFP) is defined as a plane containing the magnetic meridian of the blast point and passing through the origin, "O". The propagation plane is defined as the plane containing the propagation path and passing through the origin. A line of fundamental importance is the line-of-intersection (LOI) of the MFP and the propagation plane. The point E is the intersection of the LOI with the earth's surface. The terminal point may actually be another satellite and the direction of propagation is of no consequence, so that transmitters

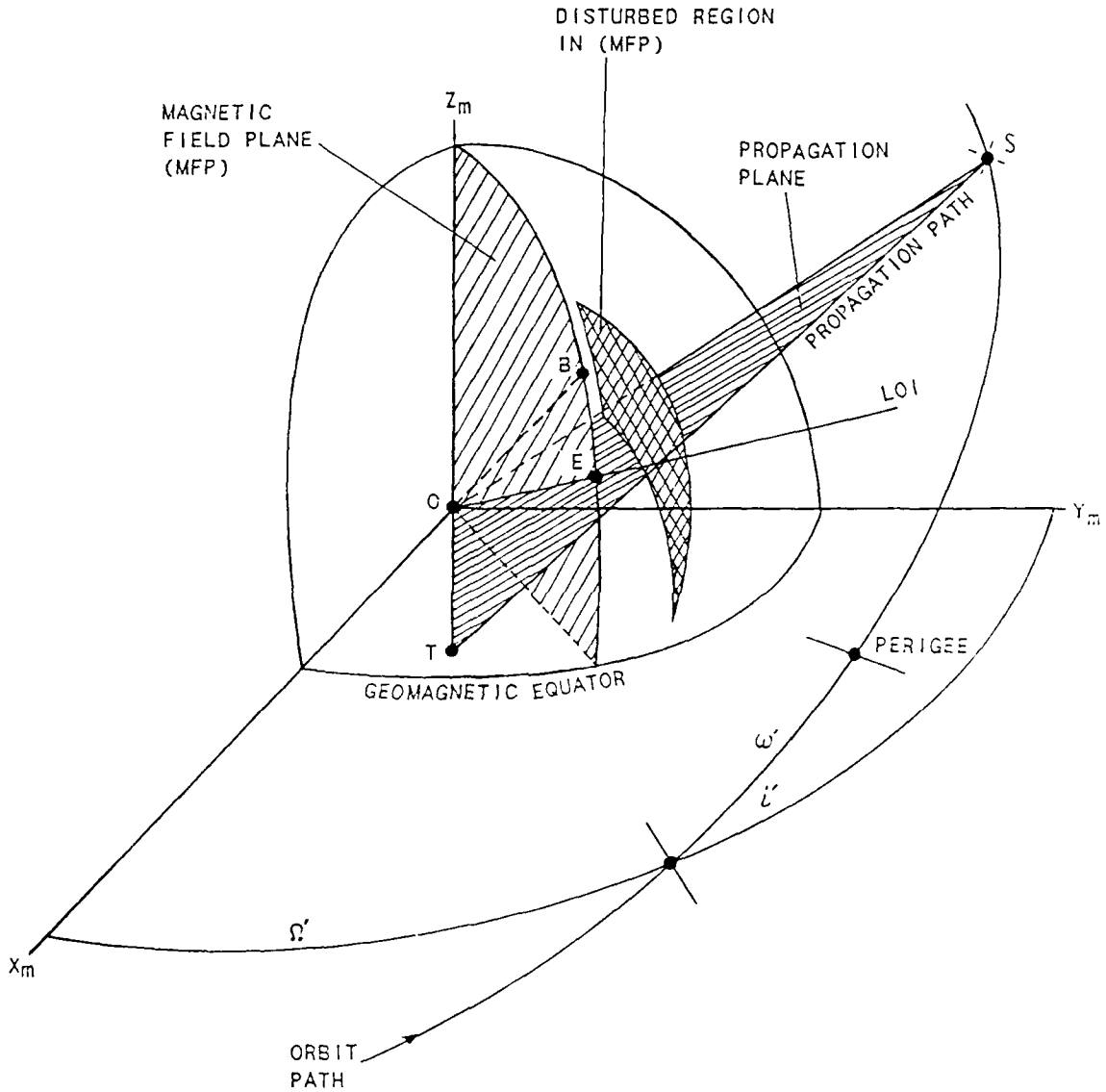

Figure 9. Geometry of a Typical Propagation Path in Geomagnetic Coordinates

or receivers, or both, may exist at any location. An important point to note from Figure 9 is that the disturbed region has no thickness except when both S and T are in the MFP. This is due to the fact that the electron density contours are specified only in the magnetic field plane. As mentioned above, the SCC will generate the contours having thickness along any propagation path by using an elliptical rotation of the MFP data.

Because the disturbed region is generally narrower, for a single detonation, across the magnetic fields, the minor axis of the rotation ellipse is taken to be normal to the MFP. In this regard, a conservative method is to use a circular rotation into the propagation plane. When the electron density contour data is stored in three-dimensions, other curve fitting methods will be adopted to determine the electron density contours in the propagation plane. The details of the various coordinate transformations required to obtain the electron density contours in the propagation plane are discussed in Appendix C. The end result is that the desired contours are expressed relative to the propagation path. An example result is shown in Figure 10.

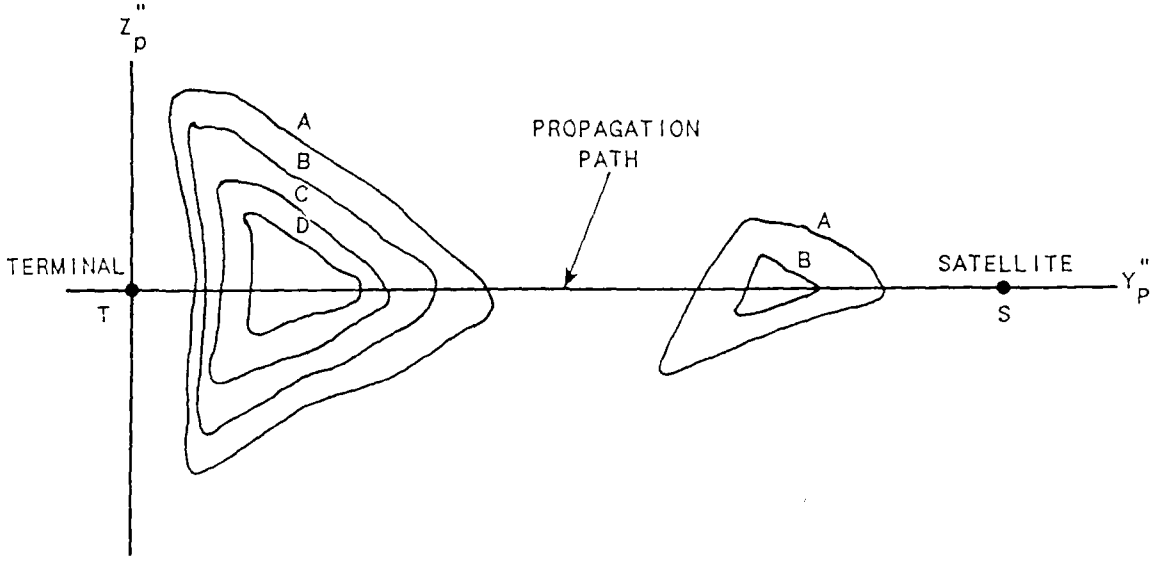

Figure 10. Example of Electron Density Contour in the Propagation Plane

The axes in Figure 10 are designated Y_p", Z_p" with the origin at the terminal point. The Y_p" axis is along the propagation path pointing towards the satellite at S. In this example, the two distinct contour segments result from the manner in which the propagation path is oriented relative to the disturbed region. This is not a typical result, but it does demonstrate the complexity of profiles along the propagation path. The axis orientation shown in Figure 10 is convenient because it simplifies the next task of the SCC, which is to compute the TEC (i.e. N_T) and the variance σ_e^2 of the electron fluctuations along the propagation path. The results, together with the determination of L_x, L_y, L_z, and L_p and the specified operating frequency, are then used to evaluate equations (1) through (6) for controlling the ACS or the host computer.

The SCC must repeat the above evaluations for each link connecting various operator specified communication platforms. The SCC must then update the results with the passage of time based upon the dynamics of platforms, the earth, and the evolving electron density structure. In addition, the SCC must control the operator's display console, depicting the geometric encounters as shown in Figure 9, and provide other useful data for a real-time assessment of the performance.

A PC, using an 80287 math coprocessor and a 10 MHz clock, requires 4.0 seconds to compute the channel parameters for a single link under the worst conditions. To relate this to the real-time parameter update rate, consider a satellite in a 1100 Km altitude circular orbit for which the orbit time is 4636 seconds. Using the criterion that the Rytov index ($\bar{\chi}^2$) is not to change by more than a factor of 3:1 between updates, the maximum update interval is 17.6 seconds. Therefore, up to four link paths can be processed by the computer in real-time. In the case of higher orbit altitudes, the maximum real-time update interval increases. For example, applying the above criterion to a 9600 Km altitude orbit, the maximum update interval becomes about 55 seconds, allowing up to 13 different links to be evaluated simultaneously in real-time. It should be pointed out that the update rate is not related to the scintillation correlation time parameter τ_0, which may

be only a few milliseconds. It is the job of the hardware channel simulator to disturb the test signal at these relatively fast rates. The SCC, on the other hand, must only update the channel parameters at a rate commensurate with a change in the parameter specification.

A. Sample SCC Results

Several example results are presented in this section to demonstrate the way in which the channel parameters affect the communication link performance. The first example represents a worst case situation, in which a reference satellite is in a polar orbit along the same meridian as the detonation. This satellite is communicating with a ground terminal directly under the blast point. There are a total of 5 orbits equally spaced around the equator with progressively staggered perigee points. All the orbits are circular polar orbits at 9600 Km altitude and each orbit contains 6 equally spaced satellites. The reference satellite is considered to be the first of 5 equally spaced satellites in orbit number 1 and is designated as (orbit, satellite) = (1,1). As the satellites travel across the sky, the SCC computes the parameters necessary to characterize the communication performance. The $\bar{\chi}^2$ parameter is illustrated in Figure 11. In this example, the $\bar{\chi}^2$ parameter is computed for each communication path between the reference satellite and the ground terminal and between its three nearest neighbors and the ground terminal. In Figure 11, the $\bar{\chi}^2$ parameter is normalized to the cube of the operating frequency, (c.f. eq. (6)).* The abscissa represents the angle from the ground terminals zenith to the reference satellite (1,1) and - 90° represents the terminal horizon when looking south. The ordinate normalization also represents the actual $\bar{\chi}^2$ index at f_c = 1 GHz and severe scintillation occurs for $\bar{\chi}^2 > 0.1$. The points at which severe scintillation occurs is indicated on the right side of Figure 11 for f_c = 1 GHz, 20 GHz, and 40 GHz. As the reference satellite

---

* These results are for $L_x = L_y = 1$ km, $L_z = 10$ Km, and the magnetic and geographic poles are colocated, i.e., $\phi_0 = 90°$, $\lambda_0 = 0°$.

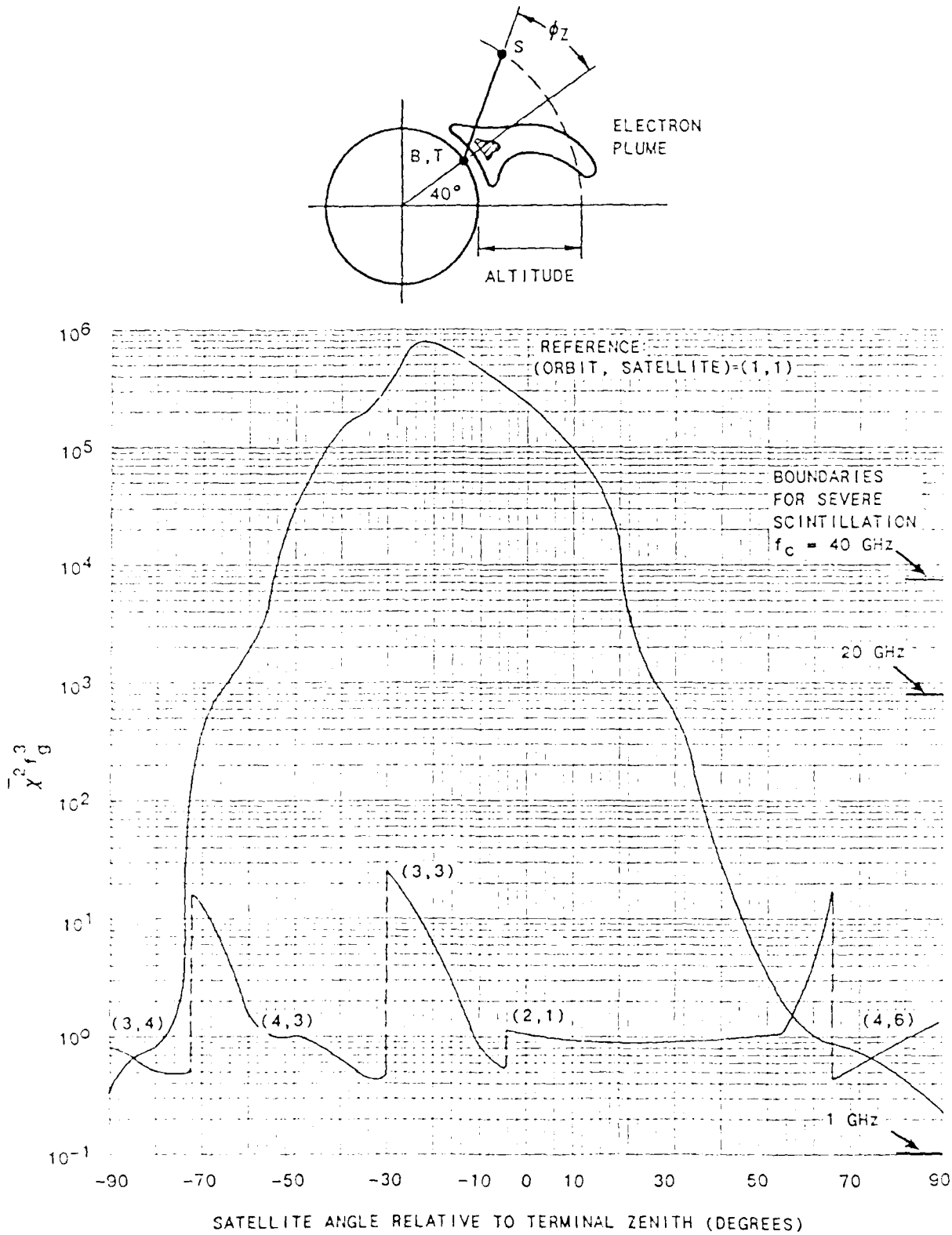

Figure 11. Scintillation Characteristics for Satellite to Ground Terminal Link

crosses the southern horizon, satellite (3,4) is the nearest of 3 neighbors having the lowest scintillation index, although severe scintillation occurs on both links at 1 GHz. In fact, severe scintillation occurs at 1 GHz for all satellites throughout the entire scenario. At 20 and 40 GHz, however, no problems have developed at this point. As the reference satellite reaches about -73°, satellite (4,3) has the lowest scintillation index of the three nearest neighbors. A satellite is dropped if it is no longer a nearest neighbor or it is no longer in view of the ground terminal. At 20 GHz, the reference satellite encounters severe scintillation between -66° and +28°, although data can be communicated through various nearest neighbors provided they are operating above 7 GHz. For this same example, Figure 12 shows the normalized signal absorption through the channel. Signal blackout will occur whenever the absorption exceeds the link design power margin. For a power margin of 3 dB, it is seen that blackout will occur between -45° and +13° for the reference satellite operating at 1 GHz. The corresponding absorption for the nearest neighbors is less than 0.1 dB. Above 2 GHz, blackout does not occur for any of the satellites.

As a second illustration of the SCC computations, consider two satellites spaced 60° apart in a circular orbit. As in the previous illustration, the orbit plane is taken to be a polar orbit along the same meridian as the detonation. The satellites travel counterclockwise along their orbit path and the leading satellite is considered to be the terminal which receives (or transmits) data from (or to) the reference satellite. In terms of the orbit and satellite designations used previously, the communication path is between satellites (1,1) and (1,2). The geometry, together with the normalized scintillation index (which is plotted as a function of the reference satellite position angle, ϕ_S), is depicted in Figure 13. The results are shown for two different satellite altitudes, 1100 km and 9600 km. For the 9600 km orbit, the communication link intersects the upper edges of the electron plume, although no scintillation is encountered at the typical crosslink frequency of 60 GHz. The 1100 km orbit exhibits two distinct peaks in the scintillation index. These peaks arise because the communication path intersects the electron plume in the region of the highest

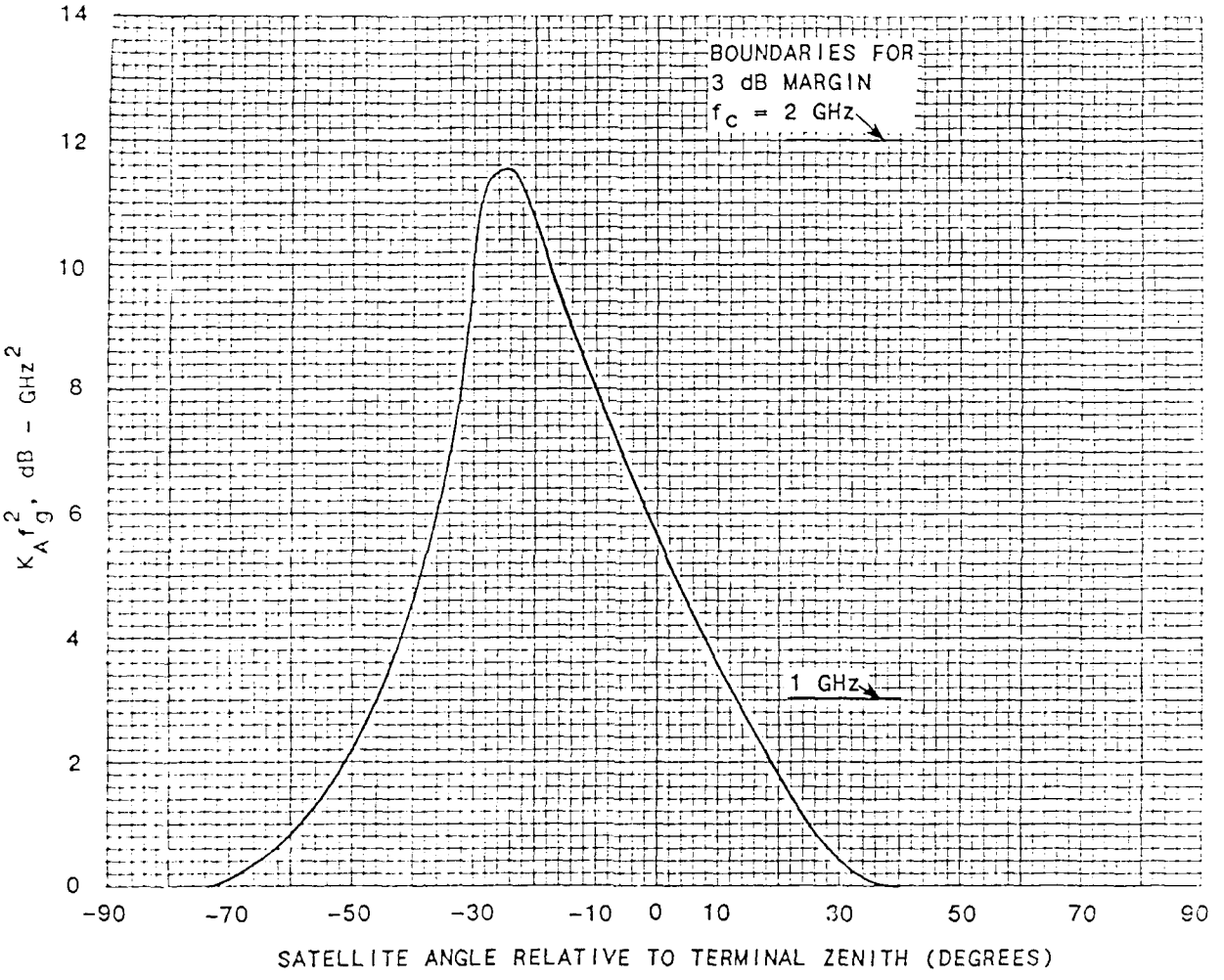

Figure 12. Absorption Characteristics for Satellite to Ground Terminal Link

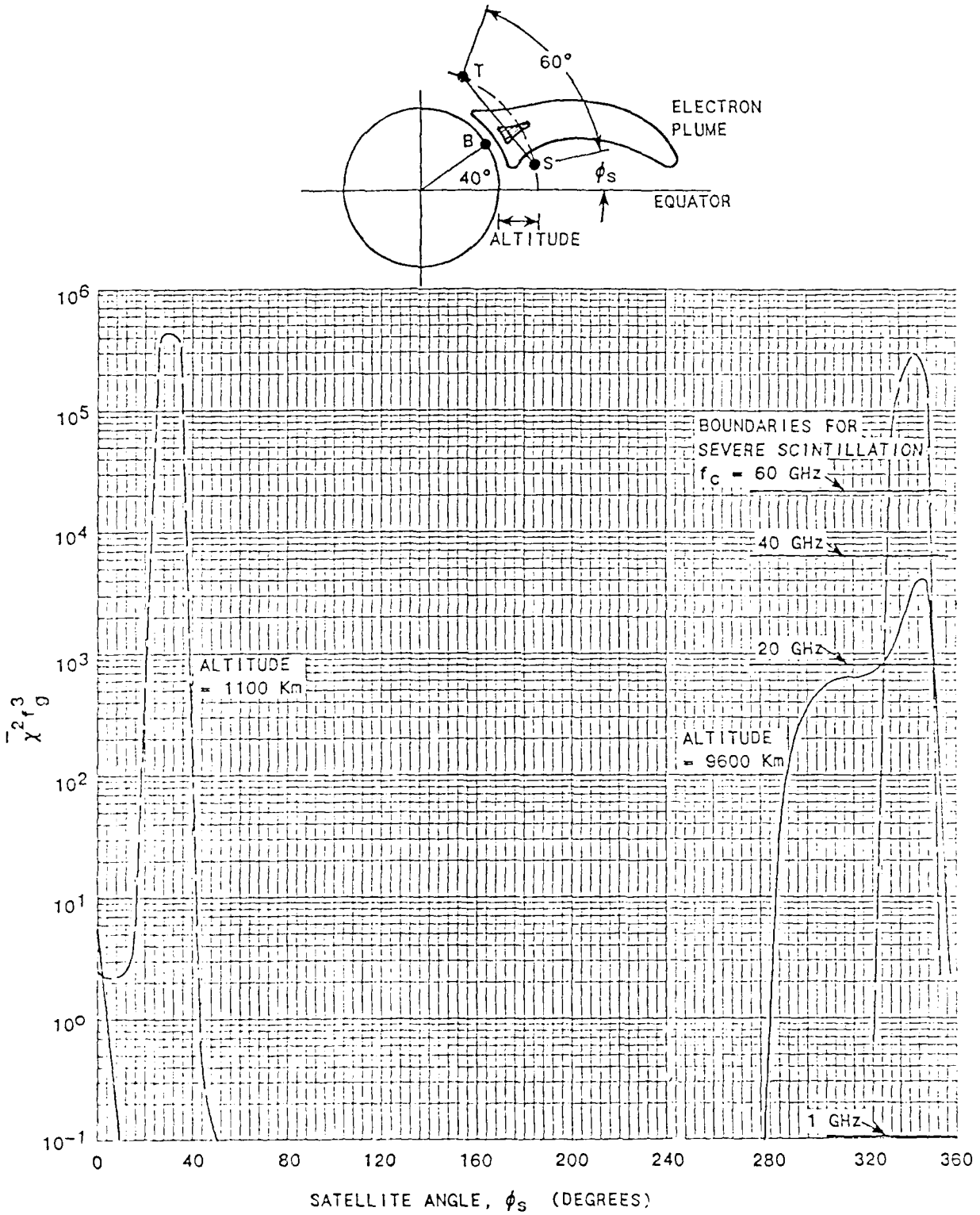

Figure 13. Scintillation Characteristics for Satellite Cross Links

concentration of electrons. This region is illustrated by the darkened region of the plume in Figure 13. The relatively low scintillation index, around zero degrees, which distinguishes the two peaks, results because the communication path intersects the plume under the highly disturbed region. The normalized absorption factor $K_A f_g^2$ has a similar relationship with ϕ_s in that peaks in K_A correspond to peaks in $\bar{\chi}^2$. For the 9600 km altitude situation, the maximum normalized absorption is 0.8 dB - GHz^2 and occurs at $\phi_s \approx 347°$. This corresponds to 0.8 dB at 1 GHz and, above about 3 GHz, the absorption is less than 0.1 dB. For the 1100 km altitude orbit, the normalized absorption has two peaks: 8.9 dB - GHz^2 at 34.3° and 6.7 dB - GHz^2 at 347°. For operating frequencies above 9.5 GHz, these results correspond to less than 0.1 dB absorption.

Although very informative, the results of these illustrations are not an end in themselves. The principle purpose of the numerical values of the various parameters is to control the ACS or the host computer software in the evaluation of equipment, software, and concepts for the SDI program. On the other hand, plots similar to those in Figures 11-13 will be displayed on the operator's console to provide insight into the channel conditions during the evaluations.

4.0 CONCLUSIONS

The real-time stressed channel simulator (RTSCS) will be a valuable asset to the SDI program in assessing BM/C^3 hardware, software, and conceptual designs in a stressed communication environment. Of particular importance is the utility of the RTSCS in supporting the objectives of the National Test Facility (NTF) and various remote facilities which form the National Test Bed (NTB). In this regard, the RTSCS will provide an important vehicle to compare, evaluate, and test alternative system and BM/C^3 architectures for defense against ballistic missiles. In addition to C^3 applications, which have been emphasized in this report, the RTSCS can be used in the evaluation of radar and active sensor signals in a stressed environment.

The two principal configurations of the RTSCS are referred to as the Experimental Test Configuration and the Simulation Test Configuration. In the Experimental Test Configuration, the RTSCS controls the hardware channel simulator for evaluating the impact of stressed communication links on various hardware equipment, either in a laboratory environment or in an "in-circuit" setup. The "in-circuit" setup allows for the RF signal from (or to) a satellite to be disturbed in a controlled manner. In the Simulation Test Configuration, the RTSCS inputs data to a host computer for the simulation of stressed channel affects on software models of equipment or networks. In this configuration, the processing is performed at a speed compatible with the host computer and may not be in real-time.

The common denominator in both configurations is the Stressed Channel Computer (SCC). The SCC is a personal computer (PC) with software developed under this research effort. The PC computes the necessary channel parameters for the ACS or as input data for the host computer. In addition, the SCC provides a dynamic graphical display of the scenario and selected numerical graphs so that the operator can assess various test results during the testing. In setting up a test scenario, the operator must identify the yield of the nuclear detonation, the location of the blast point, and the

communication links which are to be evaluated. The nuclear detonation characteristics identify a library of data files for use by the PC. However, if files for a particular event do not exist, they must be created using other computer codes* which do not run in real-time. The communication links can be selected from any combination of ground, airborne, or satellite platforms. In a severe channel environment, the PC requires four seconds to compute the link parameters necessary to control the ACS. For low orbiting satellites, which require the shortest update interval, the PC has time to compute parameters for up to four individual links. For orbit altitudes greater than 9600 Km, the PC can compute the parameters for more than 13 individual links.

The Phase I research effort discussed in this report provides an important first step in characterizing many of the concepts involving the RTSCS. Throughout this research, dialogues with Department of Defense (DoD) agencies and contractors provided direction towards real applications. The Phase II research will complete these first steps and result in a fully operational RTSCS. The major areas of focus in the Phase II research are: 1) interface the SCC with a hardware channel simulator and demonstrate the disturbances to a test signal (Two large existing channel simulators are the Advanced Channel Simulator (ACS) and the Nuclear Effects Link Simulator (NELS-II)), 2) build or purchase a low cost flat fade (non-frequency selective) hardware simulator, 3) develop a user friendly data input capability for the SCC, 4) expand the capabilities of the real-time graphical display and include split screen depiction of scenario graphics and the graphing of selected channel parameters, 5) expand the nuclear scenario data base, and 6) refine and extend the signal processing functions within the SCC to include three-dimensional electron density data profiles. The refinements will include curve fitting in time and space to result in smooth transitions between and within the stored data files.

---

* MICE and SCENARIO are computer codes developed under DNA sponsorship for characterizing the nuclear disturbed region.

REFERENCES

[1] Technical Requirements For National Test Bed (NTB) Integration, NTB Joint Program Office, P19628-87-R-0005, May 29, 1987.

[2] A.W. Wernik and C.H. Liu, "Ionospheric irregularities causing scintillation of GHz frequency radio signals," J. Atmospher. Terrestr. Phys., vol. 36, pp. 871-879, 1974.

[3] C.L. Refenach, "Ionospheric scintillation by a random phase screen: Spectral approach," Radio Sci., vol. 10, No. 2, pp. 155-165, Feb. 1975.

[4] W.S. Knapp and K. Schwartz, Aids for the study of electromagnetic blackout, General Electric - TEMPO, Rep. DNA 3499H, Feb 1975.

[5] R.W. Hendrick, Propagation of microwave satellite signals through striated media. Mission Res. Corp., Rep. DNA 4412T, MRC-R-334, Sept 1977.

[6] D.L. Knepp, Multiple phase-screen propagation analysis for defense satellite communications system, Mission Res. Corp., Rep. DNA 4424T, MRC-R-332, Sept. 1977.

[7] L.A. Wittwer, The propagation of satellite signals through turbulent media, Air Force Weapons Lab., Rep. AFWL-TR-77-183, Jan. 1978.

[8] ———, Radio wave propagation in structured ionization for satellite applications, Defense Nuclear Agency, Rep. DNA 5304D, Dec. 1979.

[9] ———, A trans-ionospheric signal specification for satellite C^3 applications, Defense Nuclear Agency, presented at the 1980 Wescon Professional Program, Sept. 1980, paper 5/2.

[10] R.L. Bogusch, F.W. Guigliano, D.L. Knepp, A.H. Michelet, "Frequency selective propagation effects on spread-spectrum receiver tracking," Proc. IEEE, vol. 69, pp. 787-796, July 1981.

[11] K.C. Yeh, C.H. Liu, "Radio Wave Scintillations in the Ionosphere, Proc." IEEE, Vol. 70, pp. 324-360, April 1982.

[12] R.W. Middlestead, R.E. LeLevier, M.D. Smith, "Satellite Crosslink Communications Vulnerability in a Nuclear Environment," IEEE Journal on Selected Areas in Communication, Vol. SAC-5, pp. 138-145, Feb. 1987.

APPENDIX A

SATELLITE ORBITS

The satellite orbits used in this report are based on the two-body problem stated by Sir Isaac Newton. The detailed computations are based upon Newton's three laws of motion and Kepler's laws of planetary motion. For further elaboration on Newton's and Kepler's laws and subsequent material discussed in this appendix, the reader is referred to reference A1. When many earth satellites are considered, the mass of each satellite is so small relative to that of the earth that the many-body problem is appropriately treated as many two-body problems. In applying Newton's laws, the earth's gravitational field is assumed to control the orbit of the satellite with the earth and satellite represented by point masses. As such, several other influences are neglected: (1) second and higher order effects when the earth is not considered to be a point source, (2) the gravitational attractions of the sun, moon, and planets, (3) the earth's atmosphere, (4) the earth's magnetic field, (5) solar radiation, and (6) the influence of charged and uncharged particles. Neglecting these secondary effects is certainly justified when one considers that the primary investigation involves examining communication link characteristics between widely separated satellites. Therefore, small and slowly varying changes in the satellite orbit will not significantly influence the communication links. In the context of the above discussion, Kepler's first law can be applied to earth satellites: the orbit of each satellite is an ellipse with the earth at one focus.

The orbit and position of an earth satellite are described in terms of six orbital elements. The first three are the angular parameters Ω, i, and ω, which fix the orbit plane relative to the geocentric coordinates. The next two parameters are designated "a" and "e" and denote semi-major axis and the eccentricity of the elliptical orbit path. These two parameters determine the size and shape of the orbit. The sixth parameter, "τ", is the time of perigee passage, which, together with the absolute time, determines the position of the satellite in its orbit. These parameters are depicted in Figure A1.

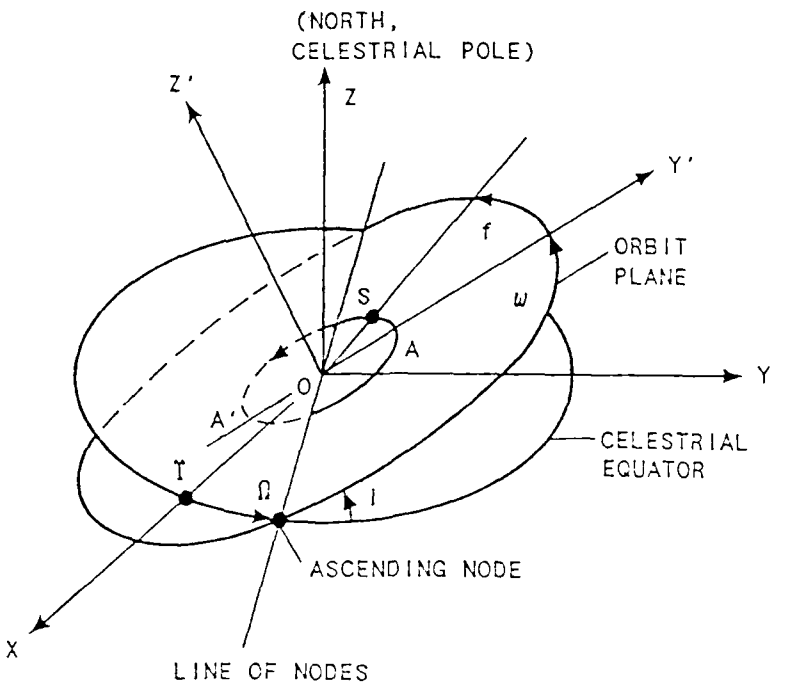

a) Orbit Relative to Geocentric Coordinates

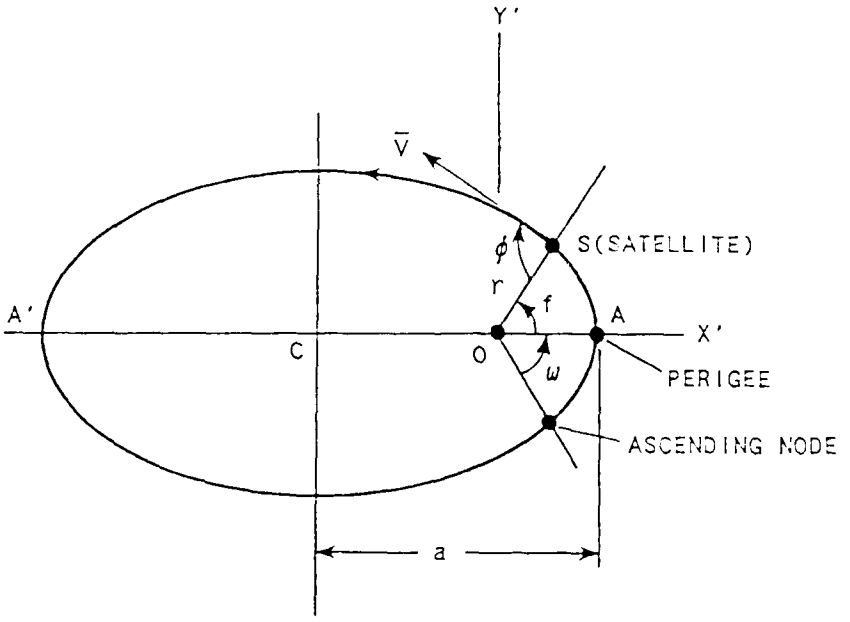

b) Satellite Orbit Path

Figure A1. Elliptical Satellite Orbit and Orbital Parameters

The celestrial equator, shown in Figure (A1a), represents the projection of the earth's equator onto the celestrial sphere. The celestrial sphere is a fictional sphere surrounding the earth, on the inside of which the stars and other heavenly bodies are projected. The point "O" denotes the origin of the geocentric coordinates, the X-axis of which passes through the First Point of Ares (♈) or the vernal equinox. The vernal equinox is the reference point chosen to establish absolute time. Using Greenwich Mean Time (G.M.T.) or Universal Time (U.T.), one tropical year is defined as the interval between successive passages of the sun through the vernal equinox. A 24-hour day in G.M.T. begins when it is mean midnight at the Greenwich meridian. To account for longitudes around the earth, civil days are defined when mean midnight occurs over meridians spaced 15° (1 hour) around the surface of the earth. This division results in Stand Time (S.T.) zones with the Greenwich Zone having bounding meridians 0^h30^mW and 0^h30^mE. The relation between G.M.T. and S.T. is

$$\text{G.M.T.} = \text{S.T.} + \text{longitude} \tag{A-1}$$

where the longitude of the meridian is added when west and subtracted when east. The ascending node is the point at which the orbit crosses the celestrical equator as the satellite passes into the northern celestrical hemisphere. The angle Ω is the right ascension of the ascending node, i is the inclination of the orbit plane, and ω is the longitude of perigee. When the inclination is 0°, the satellite is in an equatorial orbit and when it is 90°, the satellite is in a polar orbit. Using these angles, the coordinates of satellite orbit plane (X',Y',0) are translated into the geocentric coordinates using the relationship

$$\begin{bmatrix} X \\ Y \\ Z \end{bmatrix} = \begin{bmatrix} a_{11} & a_{22} \\ a_{21} & a_{22} \\ a_{31} & a_{32} \end{bmatrix} \begin{bmatrix} X' \\ Y' \end{bmatrix} \tag{A-2}$$

$$a_{11} = \cos(\Omega)\cos(\omega) - \sin(\Omega)\sin(\omega)\cos(i)$$

$$a_{12} = \cos(\Omega)\sin(\omega) - \sin(\Omega)\cos(\omega)\cos(i)$$

$$a_{21} = \sin(\Omega)\cos(\omega) + \cos(\Omega)\sin(\omega)\cos(i) \qquad \text{(A-3)}$$

$$a_{22} = -\sin(\Omega)\sin(\omega) + \cos(\Omega)\cos(\omega)\cos(i)$$

$$a_{31} = \sin(\omega)\sin(i)$$

$$a_{32} = \cos(\omega)\sin(i)$$

To account for the earth's rotation with the passage of time, the geocentric coordinates (X,Y,Z) are rotated into the earth stationary geocentric coordinates (X_e, Y_e, Z_e) as

$$\begin{bmatrix} X_e \\ Y_e \\ Z_e \end{bmatrix} = \begin{bmatrix} \cos(\theta(t)) & \sin(\theta(t)) & 0 \\ -\sin(\theta(t)) & \cos(\theta(t)) & 0 \\ 0 & 0 & 1 \end{bmatrix} \begin{bmatrix} X \\ Y \\ Z \end{bmatrix} \qquad \text{(A-4)}$$

where

$$\theta(t) = 2\pi \left[\frac{t}{T_d} \right] \qquad \text{(A-5)}$$

and T_d represents the 24 hour duration of a mean solar day expressed in the appropriate units of time.

Referring to Figure A1b, the equation for the position of the satellite, S, in the elliptical orbit, expressed in terms of the polar coordinates (r,f) is

$$r = \frac{a\,(1 - e^2)}{1 + e\cos(f)} \qquad \text{(A-6)}$$

The ellipse is horizontally symmetrical about the X' axis and vertically symmetrical about a vertical axis passing through the point C. The semi-major axis, a, is defined as being equal to the length CA = CA' and the eccentricity, e, is defined as the ratio CO/OA. When e = 0, the satellite is in a circular orbit. The time for the satellite to complete one orbital revolution is given by

$$T = 2\pi\sqrt{\frac{a^3}{G(M_e+m_s)}} \qquad \text{(A-7)}$$

where $G = 6.668 \times 10^{-8}$ dyn-cm^{2}gm^{-2} is the constant of universal gravitation, $M_e = 5.98 \times 10^{27}$ gm is the earth's mass, and m_s is the mass of the satellite. Since typically $m_s \ll M_e$ and the satellite mass can be neglected in computing T. The angle f is called the true anomaly of the satellite and the satellite coordinates are given by

$$x' = r\cos(f)$$

$$y' = r\sin(f) \qquad \text{(A-8)}$$

Figure A1b also shows the tangential velocity, V, of the satellite which is at an angle ϕ relative to the radius r. In terms of the satellite coordinates, the velocity components are given by

$$V_x = -V \cos(\phi - f)$$

$$V_y = V \sin(\phi - f) \qquad \text{(A-9)}$$

In evaluating equations (A-8) and (A-9), the parameters r, f, V, and ϕ must be determined. The solution involves defining the mean anomaly, M, and the eccentric anomaly, E, which are used as intermediate parameters. The details for the following computations are found in reference A1. First, calculate the mean anomaly as

$$M = \frac{2\pi}{T}(t - \tau) \qquad \tau \leq t \leq \tau + T \qquad \text{(A-10)}$$

recalling that T is the mean orbital time, τ is the time of perigee passage, and t is the absolute time. The mean anomaly is used to solve for the eccentric anomaly using Kepler's equation

$$M = E - e \sin(E) \qquad \text{(A-11)}$$

This is a transcendental equation for which a variety of techniques can be used to obtain a solution. The value of r and f are now computed as

$$r = a\,(1 - e \cos(E)) \qquad \text{(A-12)}$$

$$f = 2 \tan^{-1}\left[\sqrt{\frac{1+e}{1-e}}\ \tan(E/2)\right] \qquad \text{(A-13)}$$

It is important that the proper quadrants be preserved in these computations. Substitution of equation (A-13) into equation (A-6) to verify the value of r provides a good check. The velocity equations are computed using

$$V = \left[G\,(M_e + m_s) \left[\frac{2}{r} - \frac{1}{a} \right] \right]^{1/2} \qquad \text{(A-14)}$$

and

$$\phi = \sin^{-1} \left[\left[\frac{a^2(1 - e^2)}{r(2a - r)} \right]^{1/2} \right] \qquad \text{(A-15)}$$

Considerable simplification occurs for a circular orbit. Under this condition, $e = 0$, $f = M = E$, $r = R$ = constant, the desired parameters are evaluated as

$$\left.\begin{aligned} f &= \frac{2\pi}{T}(t - \tau) \\ V &= \left[\frac{G(M_e + m_s)}{R} \right]^{1/2} \\ \phi &= 90 \text{ degrees} \end{aligned}\right\} \text{ for circular orbits} \qquad \text{(A-16)}$$

APPENDIX B

TRANSFORMATION BETWEEN GEOGRAPHIC AND GEOMAGNETIC COORDINATES

This appendix discusses the transformations required to convert from the geocentric spherical coordinate system (R,ϕ,λ) to the geomagnetic coordinate system (R,Φ,Λ). The geocentric and magnetic radii are both taken to be equal to R. For points on the earth's surface, assumed to be spherical, R is equal to the mean earth radius R_e = 6378.12 Km. The plane through the center of the earth and perpendicular to the axis connecting the north and south geographic poles is the geographic equatorial plane and the circle formed by its intersection with the earth's surface is the geographic equator. The geographic latitude, ϕ, is measured in degrees north (positive) or south (negative) from the geographic equator. The geographic longitude λ is measured east (positive) from the Greenwich meridian. The magnetic field is assumed to result from a geocentric dipole the axis of which intersects the earth's surface at the north and south magnetic poles. The north (or Boreal) magnetic pole is at 78.6°N, 69.8°W and the south (Austral) magnetic pole is at 78.6°S, 290.2°E. The plane through the center of the earth and perpendicular to the dipole axis is the dipole equatorial plane and the circle formed by its intersection with the earth's surface is the dipole equator. The dipole latitude, Φ, is taken in degrees north (positive) or south (negative) from the dipole equator. The dipole longitude, Λ, is measured east (positive) from the dipole meridian passing through the magnetic poles and the south geographic pole. These relationships are depicted in Figure B1, where P and K denote the north geographic and magnetic poles, respectively. The north magnetic pole is expressed in terms of the geographic latitude ϕ_o = 78.6°N and longitude λ_o = 69.8°W. The point, X, is an arbitrary point identified in terms of the geographic coordinates (ϕ,λ) and it is desired to transform X to the magnetic coordinates (Φ,λ). The angles λ_o, λ, and Φ are measured east from the respective meridians.

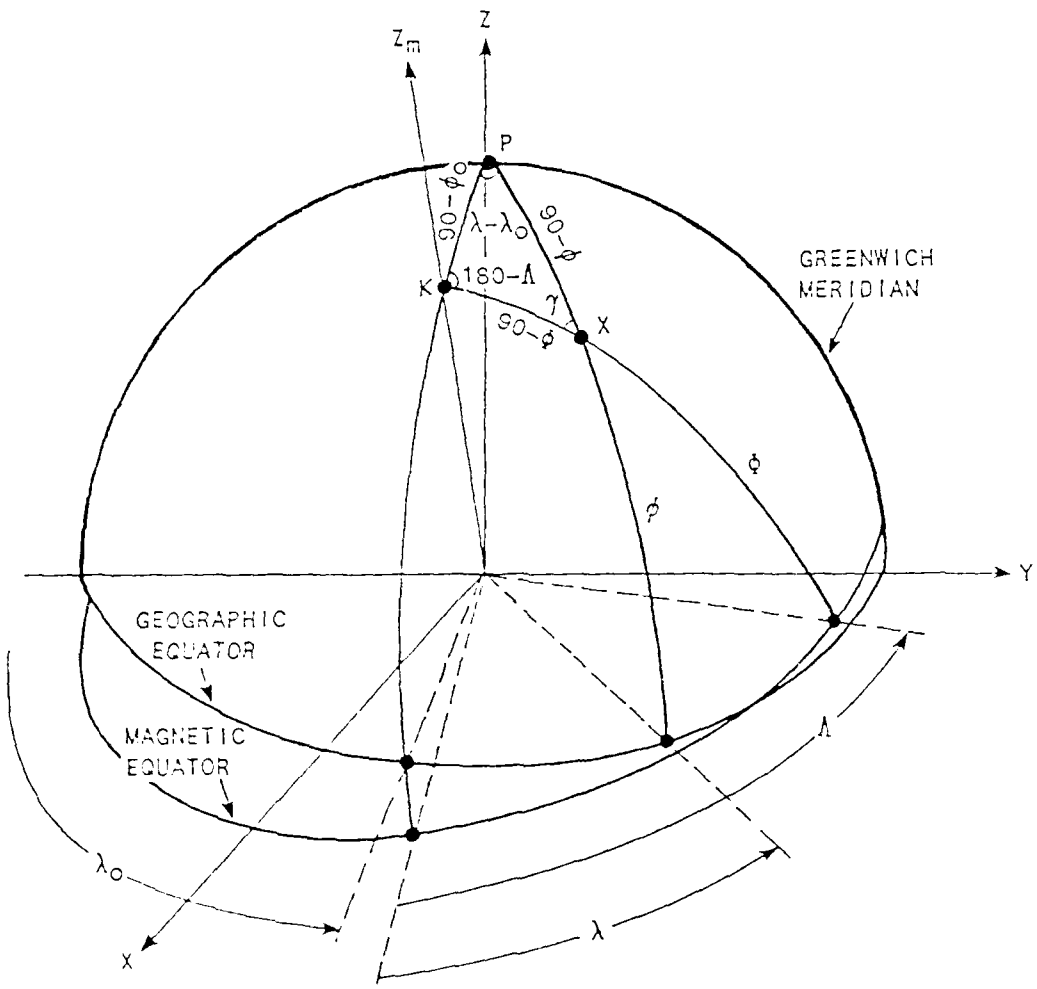

Figure B1. Relationship Between Geographic and Geomagnetic Coordinates

a. Geographic-to-Geomagnetic Transformation

When the geographic coordinates (ϕ,λ) of the point X, shown in Figure B1, are given, the geomagnetic coordinates (Φ,Λ) are computed using spherical trigonometry with the aid of Figure B1. To obtain the geomagnetic latitude, Φ, of the point X, the law of cosines for spherical trigonometry is applied to the spherical triangle PKX in Figure B1. The result is

$$\cos(90-\Phi) = \cos(90 - \phi_0)\cos(90 - \phi) + \sin(90 - \phi_0)$$
$$\sin(90 - \phi)\cos(\lambda - \lambda_0) \qquad \text{(B-1)}$$

which simplifies to

$$\sin(\Phi) = \sin(\phi_0)\sin(\phi) + \cos(\phi_0)\cos(\phi)\cos(\lambda - \lambda_0) \qquad \text{(B-2)}$$

The magnetic latitude is then simply given by

$$\Phi = \arcsin(\sin(\Phi)) \qquad \text{(B-3)}$$

In a similar way, the geomagnetic longitude is obtained by applying the law of sines with the result

$$\frac{\sin(180 - \Lambda)}{\sin(90 - \phi)} = \frac{\sin(\lambda - \lambda_0)}{\sin(90 - \Phi)} \qquad \text{(B-4)}$$

which simplifies to

$$\sin(\Lambda) = \frac{\cos(\phi)\sin(\lambda - \lambda_0)}{\cos(\Phi)} \qquad \text{(B-5)}$$

At this point, the geomagnetic longitude could be determined as $\Lambda = \arcsin(\sin(\Lambda))$ by using

$$\cos(\Phi) = \sqrt{1 - \sin^2(\Phi)} \qquad \text{(B-6)}$$

together with equation (B-2). However, if this approach is taken, care must be taken in determining the correct quadrant for Λ: 1) $270° < \Lambda < 360°$ for points lying in the geographic quadrant between two great circles that connect the north and south (dipole) magnetic poles and that cross the equator at 69.8°W and 159.8°W; 2) $180° < \Lambda < 270°$ for the geographic points between the two great circles that cross the equator at 159.8°W and 249.8°W; 3) $0° < \Lambda < 90°$ for the geographic points between the great circles that cross the equator at 69.8°W and 20.2°E; and 4) $90° < \Lambda < 180°$ for the points between the great circles that cross the equator at 20.2°E and 110.2°E. A simple way to resolve the quadrants in a Fortran computer program is to use the ATAN2(Y,X) intrinsic function. This can be used by first computing $\cos(\Lambda)$, as follows. Apply the law of cosines to the spherical triangle in Figure A1 solving for the side $\cos(90 - \phi)$ to obtain

$$\cos(90 - \phi) = \cos(90 - \Phi)\cos(90 - \phi_0) + \sin(90 - \Phi)\sin(90 - \phi)$$

$$\cos(180 - \Lambda) \qquad \text{(B-7)}$$

which simplifies to

$$\sin(\phi) = \sin(\Phi)\cos(\phi_0) - \cos(\Phi)\cos(\phi_0)\cos(\Lambda) \qquad \text{(B-8)}$$

Solving equation (B-8) for $\cos(\Lambda)$ gives

$$\cos(\Lambda) = \frac{\sin(\Phi)\sin(\phi_o) - \sin(\phi)}{\cos(\Phi)\cos(\phi_o)} \qquad \text{(B-9)}$$

Equation (B-2) is now substituted into (B-8) and after some manipulation the desired result is obtained as

$$\cos(\Lambda) = \frac{\sin(\phi_o)\cos(\phi)\cos(\lambda - \lambda_o) - \cos(\phi_o)\sin(\phi)}{\cos(\Phi)} \qquad \text{(B-10)}$$

Equations (A-5) and B-10) form convenient quadrature components for evaluating Λ using the ATAN2 (Y,X) function. The result is

$$\Lambda = \left[\frac{180}{\pi}\right] \text{ATAN2}\left[\cos(\phi)\sin(\lambda - \lambda_o), \sin(\phi_o)\cos(\phi)\cos(\lambda - \lambda_o) - \cos(\phi_o)\sin(\phi)\right] \qquad \text{(B-11)}$$

The factor $(180/\pi)$ converts the angle to degrees for which the values of Λ, resulting from equation B-11, are in the range $0° \leq \Lambda \leq 180°$ and $-180° \leq \Lambda \leq 0°$. The positive values correspond to east and the negative values correspond to west magnetic longitude relative to the magnetic meridian.

b. Geomagnetic-to-Geographic Transformation

When given the geomagnetic coordinates (Φ, Λ) of the point X, the geographic coordinates (ϕ, λ) are computed using spherical trigonometry with the aid of Figure B1. The procedures are similar to that described above in determining Φ and Λ and, therefore, only the key results are given. First, from the law of cosines, the geographic latitude is given by

$$\phi = \arcsin(\sin(\phi)) \tag{B-12}$$

where

$$\sin(\phi) = \sin(\Phi)\sin(\phi_0) - \cos(\Phi)\cos(\phi_0)\cos(\Lambda) \tag{B-13}$$

Using the law of sines, $\sin(\lambda - \lambda_0)$ is found to be

$$\sin(\lambda - \lambda_0) = \frac{\cos(\Phi)\sin(\Lambda)}{\cos(\phi)} \tag{B-14}$$

Applying the law of cosines to solve for $\cos(\lambda - \lambda_0)$ gives

$$\cos(\lambda - \lambda_0) = \frac{\sin(\Phi) - \sin(\phi_0)\sin(\phi)}{\cos(\phi_0)\cos(\phi)} \tag{B-15a}$$

$$= \frac{\sin(\Phi) + \sin(\phi_0)\cos(\Phi)\cos(\Lambda)}{\cos(\phi)} \tag{B-15b}$$

Using equations (B-14) and (B-15b), the intrinsic Fortran function, ATAN2 (Y,X), is used to determine the geographic longitude. The result is

$$\lambda = \lambda_0 + \left[\frac{180}{\pi} \right] \text{ATAN2} \left[\cos(\Phi)\sin(\Lambda),\ \sin(\Phi)\cos(\phi_0) + \cos(\phi)\sin(\phi_0)\cos(\Lambda) \right] \qquad \text{(B-16)}$$

The factor $(180/\pi)$ converts the result to degrees and positive (negative) values refer to east (west) longitude from the Greenwich meridian.

APPENDIX C

STRESSED CHANNEL COMPUTER (SCC): PROCESSING DETAILS

In this appendix, the details of the various coordinate transformations and other algorithms required to obtain the electron density characteristics along an arbitrary communication path are discussed. The SCC program starts with the electron density profiles generated from computer codes* developed largely under DNA sponsorship. The basic inputs for these codes are the location of a detonation, the yield, and details concerning the fission debris. The resulting electron plume is influenced by the geomagnetic field lines and is characterized by contours of constant electron density. The contours are usually expressed in terms of horizontal and vertical displacement relative to ground zero. In this appendix, all the input coordinate information is in terms of the magnetic dipole coordinates, for which the necessary transformations are outlined in appendix B. Although the contour data is computed in three-dimensional space, the data is stored in data files as arrays of two-dimensional profiles representing various cuts in three-dimensional space. The major role of the SCC is to reconstruct the contour data as a three-dimensional plume of electron densities and then project these contours onto a plane intersecting the plume at an oblique angle. The oblique plane is uniquely identified in that it contains a line representing the communication path and passes through the geomagnetic origin. The situation is depicted in Figure C1, where S is the location of the satellite and T is the terminal location. The lines designated as A, B, C, and D represent contours of constant electron density. Frequently, the electron densities are characterized in a single plane containing the meridian corresponding to ground zero of a detonation. In this situation,

*For example, MICE is a magnetic hydrodynamic computer code primarily for high altitude phenomonology and MR HYDE is a three-dimensional magneto-hydrodynamic computer code used for numerically investigating high-altitude nuclear weapons effects and SCENARIO provides three-dimensional electron density contours based on the yield and location of multiple nuclear detonations.

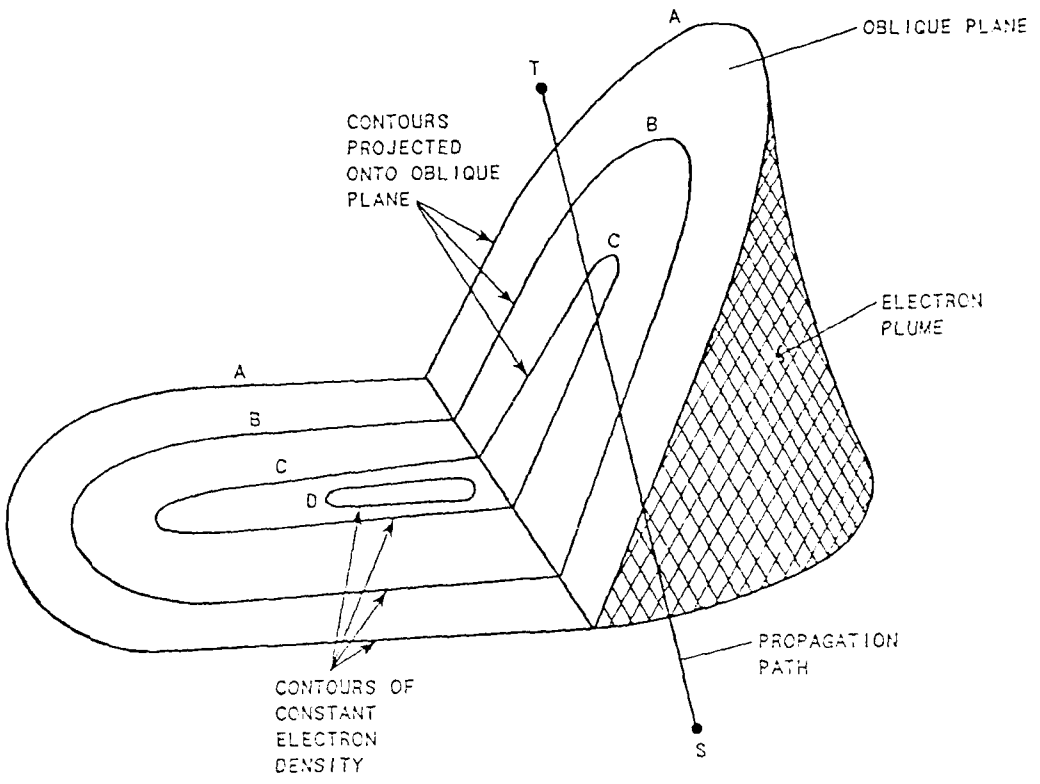

Figure C1. Projection of Electron Density Contours onto Oblique Plane Containing Propagation Path.

which is the focus of this appendix, the three-dimensional contours are reconstructed by rotating the contour data out of the specified plane using an elliptical curve fitting path. The major axis of the elliptical curve fit is aligned in the magnetic field plane (MFP) because the electron plumes are characteristically elongated in this north/south direction. In this regard, a worst case environment for a single detonation can be evaluated by using a circular rotation of the contour data. The circular case is simply a special case of the elliptical curve fit for which the major and minor axes are equal. Figure C2 depicts the situation in which the disturbed region is characterized by an electron density plume in the MFP. The points T, S, and O identify the propagation plane and the point B represents ground zero. The line-of-intersection (LOI) identifies the intersection of the MFP

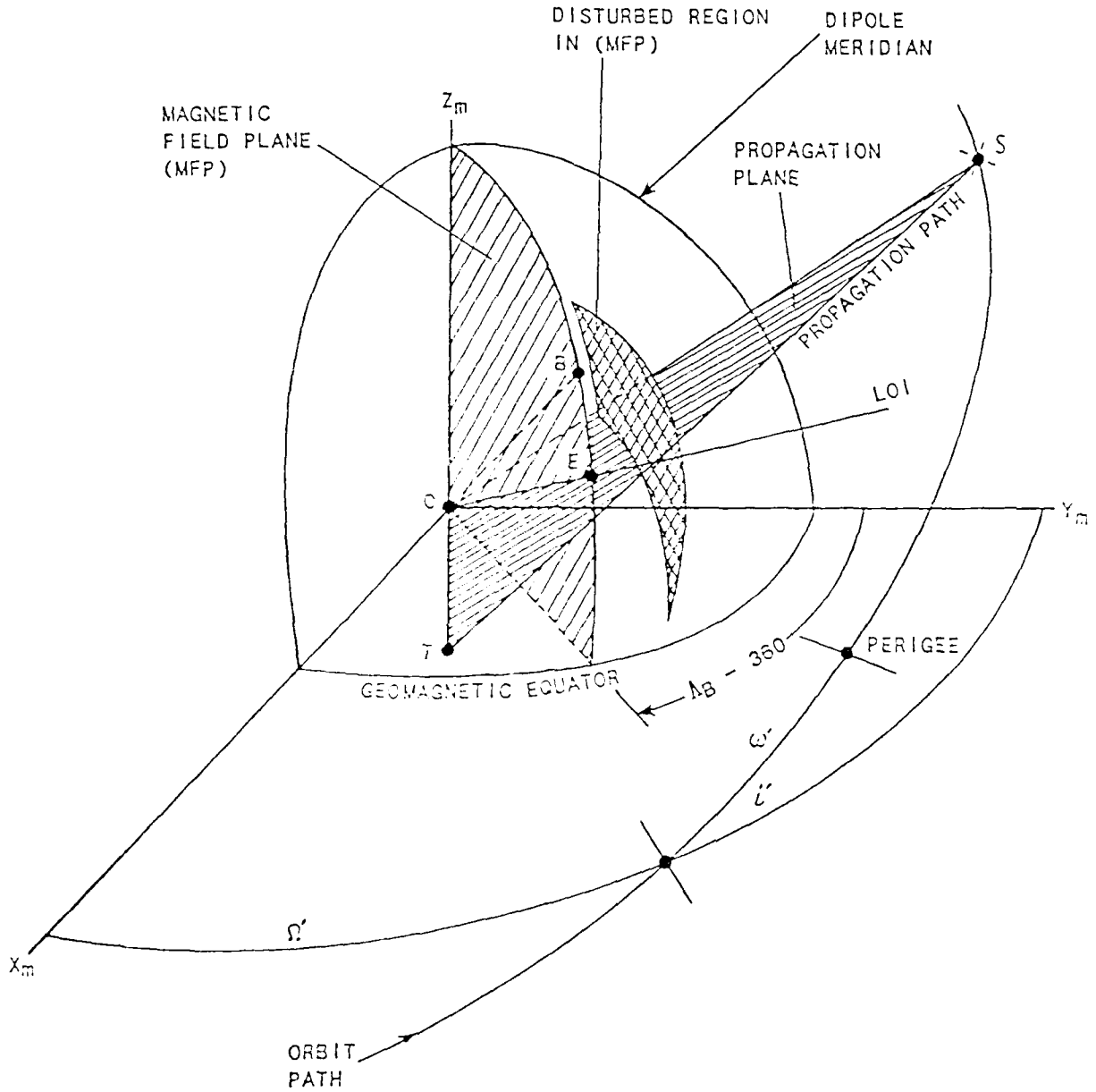

Figure C2. Geometry of a Typical Propagation Path in the Geomagnetic Coordinates

and the propagation plane and is an important reference used in the subsequent analysis. The point E is the point at which the LOI intersects earth's surface. The Y-axis of the reference coordinates is aligned with the dipole meridian. The angles Ω', ι', and ω' define the satellite orbit in the magnetic coordinates. The remainder of this appendix describes the details of various steps in obtaining the quantitative results for the total electron content (TEC) and the variance of the electron densities (σ_e^2) from which the disturbed communication path is characterized.

A. Calculation of Angles Involving the MFP and the Propagation Plane

In this section, the geometry of the points B, S, and T and the LOI is established and several key angles are computed for use in subsequent sections. With the points B, S, and T identified in terms of the corresponding geomagnetic coordinates (X_m, Y_m, Z_m), the first step in the computations is to determine the LOI. It is convenient to rotate the coordinate points through the angle Λ_B so that the MFP contains the new Y-axis as shown in Figure C3. This transformation is given by

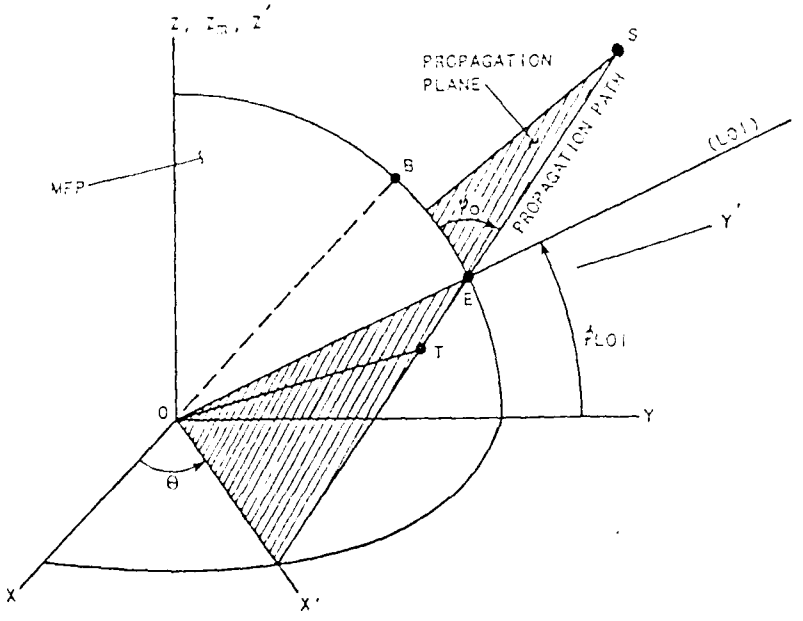

Figure C3. LOI in the (X,Y,Z) Coordinates

$$\begin{bmatrix} X \\ Y \\ Z \end{bmatrix} = \begin{bmatrix} \cos(\Lambda_B) & \sin(\Lambda_B) & 0 \\ -\sin(\Lambda_B) & \cos(\Lambda_B) & 0 \\ 0 & 0 & 1 \end{bmatrix} \begin{bmatrix} X_m \\ Y_m \\ Z_m \end{bmatrix} \tag{C-1}$$

In terms of the new coordinates, the points S and T are identified by (X_s, Y_s, Z_s) and (X_t, Y_t, Z_t), respectively. The angle ϕ_{LOI} uniquely identifies the LOI in the MFP and the angle ϕ_o is the angle between the MFP and the propagation plane. As stated above, the propagation plane contains the points S and T and passes through the geomagnetic origin. The equation for the propagation plane* is given by

$$aX + bY + Z = 0 \tag{C-2}$$

where

$$a = \frac{Z_s Y_t - Y_s Z_t}{Y_s X_t - X_s Y_t} \tag{C-3}$$

$$b = - \frac{Z_s X_t - X_s Z_t}{Y_s X_t - X_s Y_t} \tag{C-4}$$

Because the LOI is in the (Z,Y) plane, the equation for the LOI is determined by setting X equal to zero in equation (C-2). The result is

$$Z = - bY \tag{C-5}$$

from which the angle ϕ_{LOI} is found to be

$$\phi_{LOI} = -\tan^{-1}(b) \tag{C-6}$$

---

*Kells, L.M., Analytic Geometry and Calculus, Prentice-Hall, Inc., New York, Chapter 23, 1955.

The angle ψ_o will be used to determine the angle through which the contour data points must be rotated to obtain corresponding points in the propagation plane. ψ_o is computed as the angle between the vectors V_m and V_p, normal to the MFP and the propagation plane, respectively. Since the MFP is the (Z,Y) plane, the vector V_m is given by

$$V_m = 1\ \mu_x + 0\ \mu_y + 0\ \mu_z \tag{C-7}$$

where μ_x, μ_y, and μ_z are unit vectors along the indicated axis. The vector V_p is obtained from the direction cosines $\cos(\alpha) = a/d$, $\cos(\beta) = b/c$, and $\cos(\gamma) = 1/d$, with $d = \sqrt{a^2 + b^2 + 1}$, where a and b are given by equations (C-3) and (C-4). The result is

$$V_p = \left(\frac{a}{d}\right) \mu_x + \left(\frac{b}{d}\right) \mu_y + \left(\frac{1}{d}\right) \mu_z \tag{C-8}$$

so that the angle ψ_o is determined from

$$\cos(\psi_o) = V_m \cdot V_p \tag{C-9}$$

$$= \frac{a}{\sqrt{a^2 + b^2 + 1}} \tag{C-10}$$

The angle θ identifies the line in the (X,Y) plane formed by the intersection with the propagation plane. This angle is computed using equation (C-2) with $Z = 0$ and is expressed as

$$\theta = \tan^{-1}\left(\frac{-a}{b}\right) \tag{C-11}$$

B. Translation of Contour Data Points in the MFP

The contour data points are specified in the MFP in pairs in such a way that the line connecting pairs of points is normal to a line through the center of the plume. A typical pair of data points, designated as A and A', is shown in Figure C4.

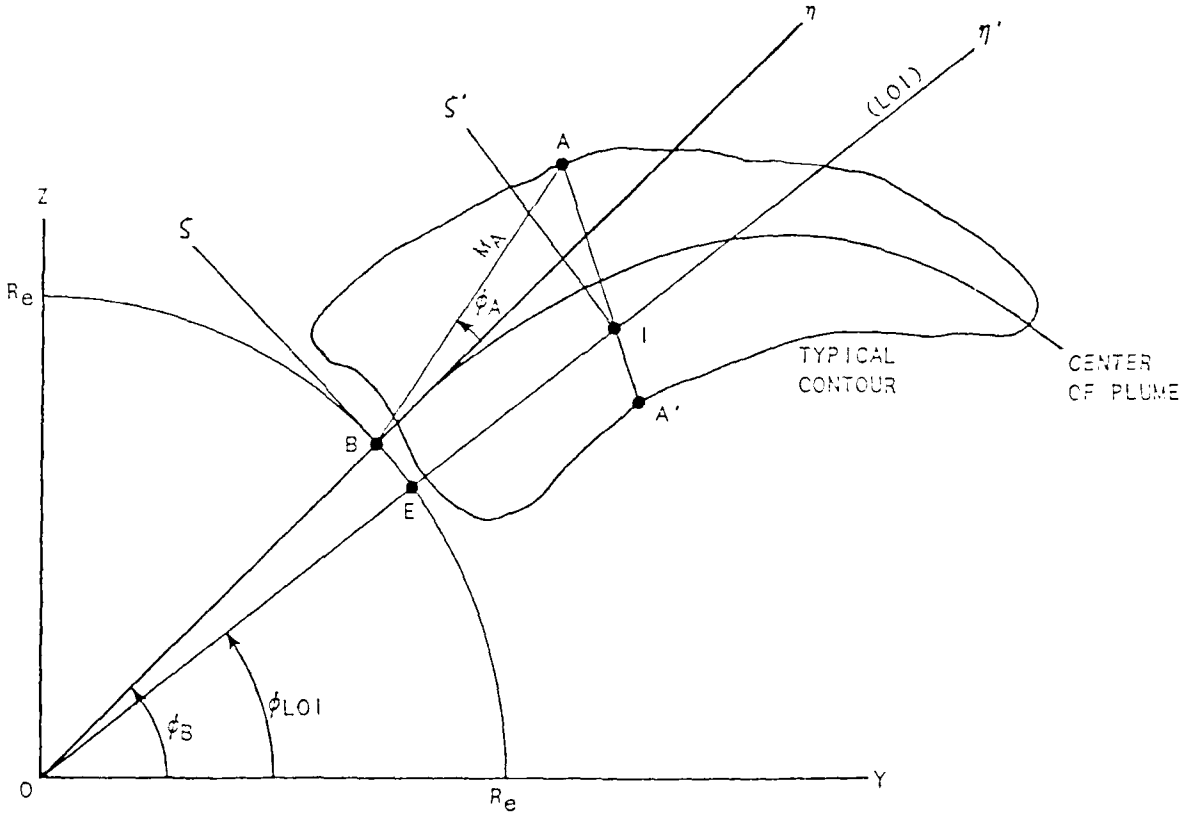

Figure C4. Geometry in the MFP

The data is stored in a file as a magnitude and phase angle relative to the ς-η axes so that for the point A, the coordinates are

$$\varsigma_A = M_A \sin(\phi_A)$$

$$\eta_A = M_A \cos(\phi_A) \qquad \text{(C-12)}$$

In terms of the Y,Z axes, the point A is expressed as

$$\begin{bmatrix} Z_A \\ Y_A \end{bmatrix} = \begin{bmatrix} \cos(\phi_B) & \sin(\phi_B) \\ -\sin(\phi_B) & \cos(\phi_B) \end{bmatrix} \begin{bmatrix} \varsigma_A \\ R_e + \eta_A \end{bmatrix} \qquad \text{(C-13)}$$

The point A' is transformed in a similar way. The rotation of the points A and A' into the propagation plane is performed relative to the point-of-intersection of the LOI and the line connecting A and A'. This intersection is the point I in Figure C4. The line connecting A and A' is expressed as

$$Z = SY + Z_o \qquad \text{(C-14)}$$

with

$$S = \frac{Z_A - Z_A'}{Y_A - Y_A'} \qquad \text{(C-15)}$$

and

$$Z_o = Z_A - SY_A \qquad \text{(C-16)}$$

The point Y_I is determined by equating equations (C-14) and (C-5) and solving for Y_I with the result

$$Y_I = \frac{-Z_o}{(S + b)} \tag{C-17}$$

and from equation (C-5)

$$Z_I = -bY_I \tag{C-18}$$

The point A, expressed by equation (C-13), is now translated to the point I and rotated through the angle ϕ_{LOI}. The result is

$$\begin{bmatrix} \eta'_A \\ \varsigma'_A \end{bmatrix} = \begin{bmatrix} \cos(\phi_{LOI}) & \sin(\phi_{LOI}) \\ -\sin(\phi_{LOI}) & \cos(\phi_{LOI}) \end{bmatrix} \begin{bmatrix} Y_A - Y_I \\ Z_A - Z_I \end{bmatrix} \tag{C-19}$$

Transforming the point A' in a similar manner, the situation is depicted in Figure C5 in terms of the $(\xi', \eta', \varsigma')$ coordinates. Figure C5 also shows the propagation plane. However, the points A and A' are in the (ς', η') plane and form an angle ϕ with the ς' axis.

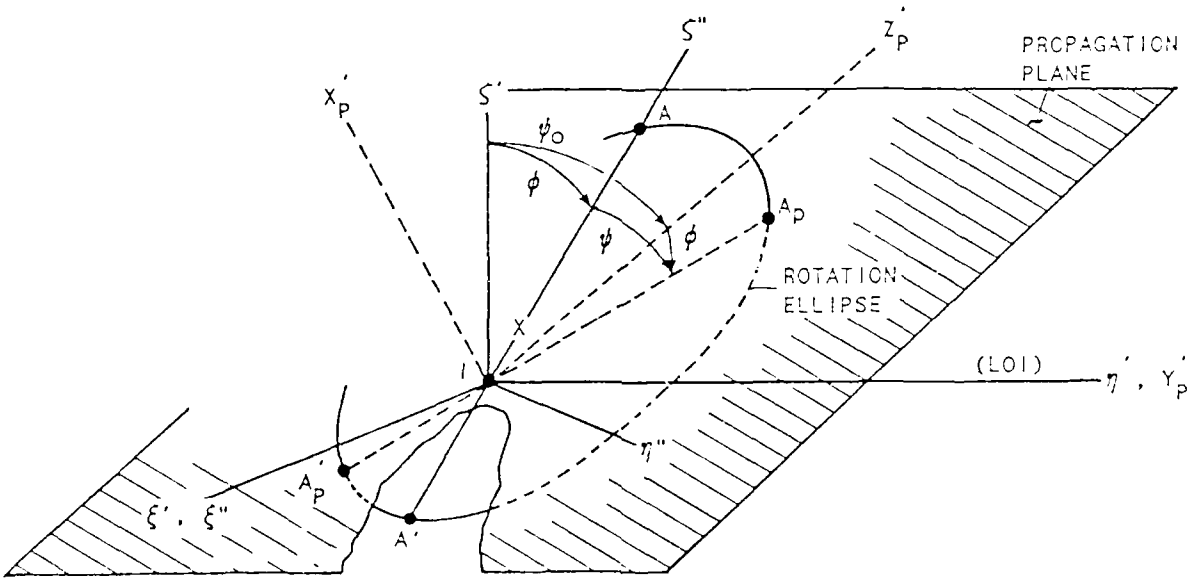

Figure C5. Typical Data Point Pair in the (ζ', η') Plane with Corresponding Points in the Propagation Plane

The point X in Figure C5 is centered between A and A' and forms the center of the rotation ellipse for determining the corresponding points A_p and A_p' in the propagation plane. The $(\xi", \eta", \zeta")$ coordinates are aligned such that the $\zeta"$ axis lies along the line from A to A' and $\xi"$ lies along the ξ' axis. The desired rotation of A and A' into the propagation plane is accomplished by rotating through the angle ψ in the $(\xi", \zeta")$ plane where ψ is determined from

$$\cos(\psi) = \sin^2(\phi) + \cos^2(\phi)\cos(\psi_o) \tag{C-20}$$

with

$$\phi = \tan^{-1}\left[\frac{\varsigma_A'}{\eta_A'}\right] \tag{C-21}$$

and cos (ψ_o) is given by equation (C-10). For the situation being considered, in which contour data is characterized only in the MFP, the rotation is readily accomplished by computing the (ξ'',ς'') coordinate solutions for the intersection of the line $A_p - A_p'$ with the rotation ellipse. The geometry is shown in Figure C6.

Referring to Figure C6, with a_e representing the length of the major axis of the rotation ellipse and ρ the ratio of the length of the minor axis to that of the major axis, the equation of the ellipse is given by

$$\frac{\xi''^2}{(\rho a_e/2)^2} + \frac{(\varsigma''-d_e)^2}{(a_e/2)^2} = 1 \tag{C-22}$$

Also, the equation of the line $A_p - A_p'$ is given by

$$\varsigma'' = K\xi'' \tag{C-23}$$

where $K = (\tan(\psi))^{-1}$.

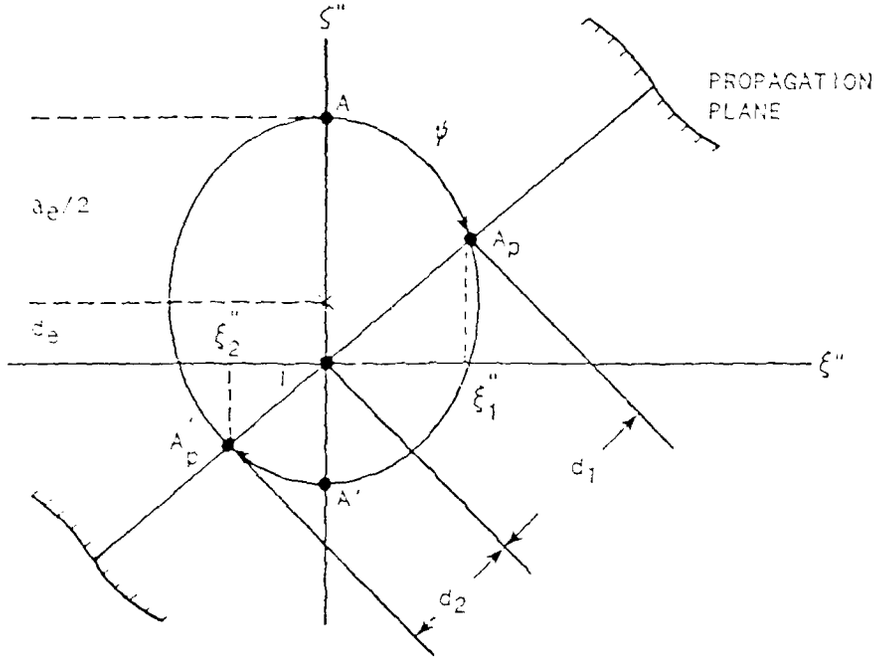

Figure C6. Rotation of A and A' into A_p and A_p' in the (ζ'', ξ'') plane.

Substituting equation (C-23) into (C-22) and solving for the points ξ_1'' and ξ_2'' gives

$$\xi_1'', \quad \xi_2'' = \frac{d_e K\rho^2 \pm \sqrt{(d_e K \rho^2)^2 - \rho^2(1 + K^2\rho^2)\ (d_e^2 - (a_e/2)^2)}}{1 + (K\rho)^2} \qquad \text{(C-24)}$$

where d_e is the displacement of the point X from the point I and is given by

$$d_e = \sqrt{\left\{\frac{\zeta_A' + \zeta_{A'}'}{2}\right\}^2 + \left\{\frac{\eta_A' + \eta_{A'}'}{2}\right\}^2} \qquad \text{(C-25)}$$

When the argument of the radical in equation (C-24) is negative, the rotation does not intersect the propagation plane and another pair of data points is considered. When a solution is found, the distances d_1 and d_2, shown in Figure C6, are computed as

$$d_1 = K \frac{\xi_1''}{\cos(\psi)}$$

$$d_2 = K \frac{\xi_2''}{\cos(\psi)} \qquad \text{(C-26)}$$

Referring to Figure C5 the points A_p and A_p' are expressed in the propagation plane coordinates (Z_p', Y_p') as

$$Z_{P1}' = d_1 \cos(\phi)$$

$$Y_{P1}' = d_1 \sin(\phi) \qquad \text{(C-27)}$$

and for the point A_P'

$$Z_{P2}' = d_2 \cos(\phi)$$

$$Y_{P2}' = d_2 \sin(\phi) \qquad \text{(C-28)}$$

At this point in the computations, the new data points are in the propagation plane relative to the (X_P', Y_P', Z_P') coordinates whose origin is at I. To simplify the numerical computations in computing TEC and σ_e^2, it is convenient to translate the origin to the terminal point T in such a way that a new Y_P'' axis is directed towards the satellite. The required transformations are discussed in the following section.

C. Transformation to the Terminal Point Origin.

Before making this final transformation, it is necessary to transform the points S, T, and I into the propagation plane. Referring to Figure C3, these points are first rotated through the angle θ, given by equation (C-11), into the (X',Y',Z') coordinates using the transformation.

$$\begin{bmatrix} X' \\ Y' \\ Z' \end{bmatrix} = \begin{bmatrix} \cos(\theta) & \sin(\theta) & 0 \\ -\sin(\theta) & \cos(\theta) & 0 \\ 0 & 0 & 1 \end{bmatrix} \begin{bmatrix} X \\ Y \\ Z \end{bmatrix} \tag{C-29}$$

In this new coordinate system, the equation of the propagation plane is expressed as

$$a'X' + b'Y' + Z' = 0 \tag{C-30}$$

where

$$a' = \frac{Z_S' Y_T' - Y_S' Z_T'}{Y_S' X_T' - X_S' Y_T'} \tag{C-31}$$

$$b' = - \frac{Z_S' X_T' - X_S' Z_T'}{Y_S' X_T' - X_S' Y_T'} \tag{C-32}$$

The Y' axis must now be rotated into the propagation plane by rotating about the X' axis through the angle β. The angle β is obtained from equation (C-30) by setting X' = 0, so that

$$\beta = \tan^{-1} (-b') \tag{C-33}$$

Therefore, the points S, T, and I must undergo the final rotation into the propagation plane coordinates given by

$$\begin{bmatrix} X_P \\ Y_P \\ Z_P \end{bmatrix} = \begin{bmatrix} 1 & 0 & 0 \\ 0 & \cos(\beta) & \sin(\beta) \\ 0 & -\sin(\beta) & \cos(\beta) \end{bmatrix} \begin{bmatrix} X' \\ Y' \\ Z' \end{bmatrix} \qquad \text{(C-34)}$$

The situation is shown in Figure C7.

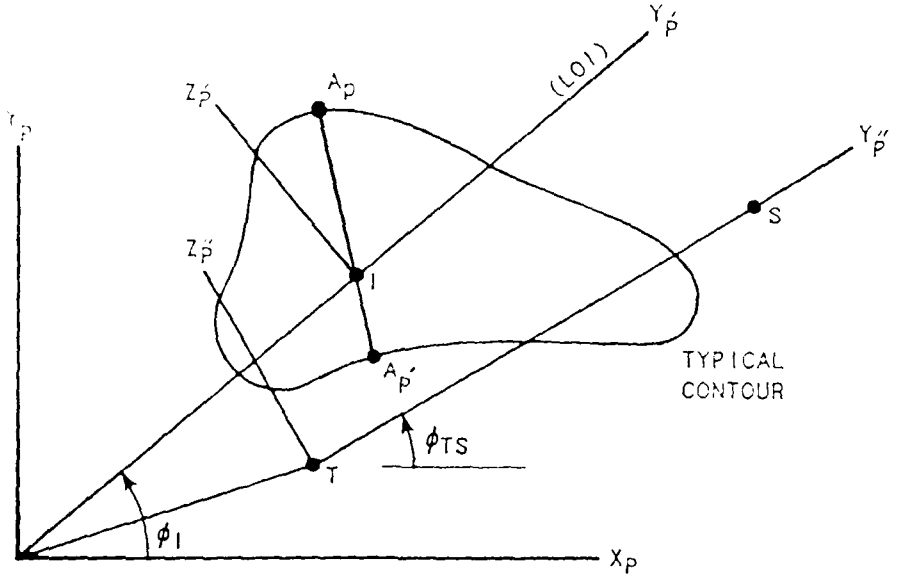

Figure C7. Geometry in the Propagation Plane

It remains to translate the points A_p and A_p', represented by equations (C-27) and (C-28), to the final coordinates (X_p'', Y_p'', Z_p'') having the origin at T. To accomplish this, the angles ϕ_I and ϕ_{TS} shown in Figure C7 are computed as

$$\phi_I = \tan^{-1}\left[\frac{Y_{PI}}{X_{PI}}\right] \tag{C-35}$$

and

$$\phi_{TS} = \tan^{-1}\left[\frac{Y_{PS} - Y_{PT}}{X_{PS} - X_{PT}}\right] \tag{C-36}$$

Using these results, the contour data point A corresponding to (Y_{P1}', Z_{P1}') is transformed into the (Z_P'', Y_P'') coordinates using the relationship.

$$\begin{bmatrix} Y_{P1}'' \\ Z_{P1}'' \end{bmatrix} = \begin{bmatrix} \cos(\phi_{TS} - \phi_I) & \sin(\phi_{TS} - \phi_I) \\ -\sin(\phi_{TS} - \phi_I) & \cos(\phi_{TS} - \phi_I) \end{bmatrix} \begin{bmatrix} Y_{P1}' \\ Z_{P1}' \end{bmatrix} + \begin{bmatrix} \cos(\phi_{TS}) & \sin(\phi_{TS}) \\ -\sin(\phi_{TS}) & \cos(\phi_{TS}) \end{bmatrix} \begin{bmatrix} X_{PT} - X_{PI} \\ Y_{PT} - Y_{PI} \end{bmatrix} \tag{C-37}$$

In a similar manner, the point A_p' is transformed to the (Z_P'', Y_P'') coordinates. In using equations (C-35) through (C-37), the points X_{PI} and Y_{PI} result from transforming the point I = (0, Y_I, Z_I), where Y_I and Z_I are given by equations (C-17) and C-18). The points (Y_{PT}, Y_{PT}) and (Y_{PS}, X_{PS}) result from the transformation of the points T = (X_T, Y_T, Z_T) and S = (X_S, Y_S, Z_S), respectively.

The processing described above represents the transformation of a single pair of data points, originally specified in the MFP, into an oblique propagation plane. To transform the entire electron density profile, the processing must be repeated for, typically, 50 data points for each of, typically, 5 electron density contours. The resulting electron density profile in the propagation plane will usually contain fewer data points because the elliptical rotation may not intersect the propagation plane. Figure C8 illustrates the complexity of the propagation plane contours which may result. In this case, the original electron density profile consisted of 5 individual contours nested one within the other.

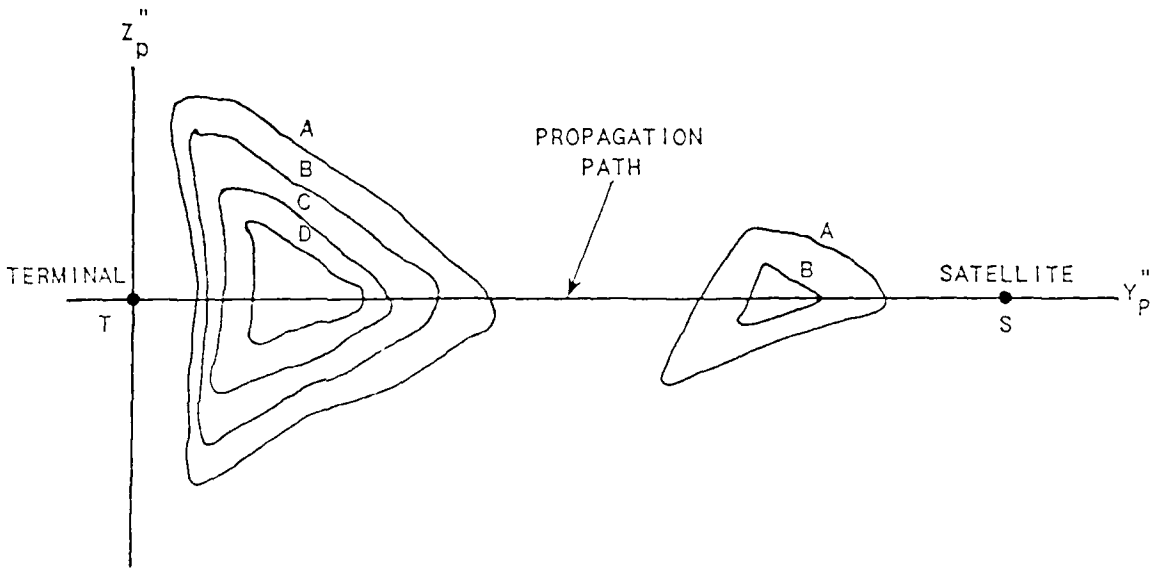

Figure C8. Example of Electron Density Contour in the Propagation Plane

Transforming the results into the (Z''_p, Y''_p) coordinates, as illustrated in Figures C7 and C8, greatly simplifies the numerical integration of the electron densities along the propagation path in the computation of TEC. Also, the variance σ_e^2, of the electron densities is related to the maximum of the electron densities which intercept the propagation path. Therefore, the computation of σ_e^2 is also straightforward in the (Z''_p, Y''_p) coordinates.

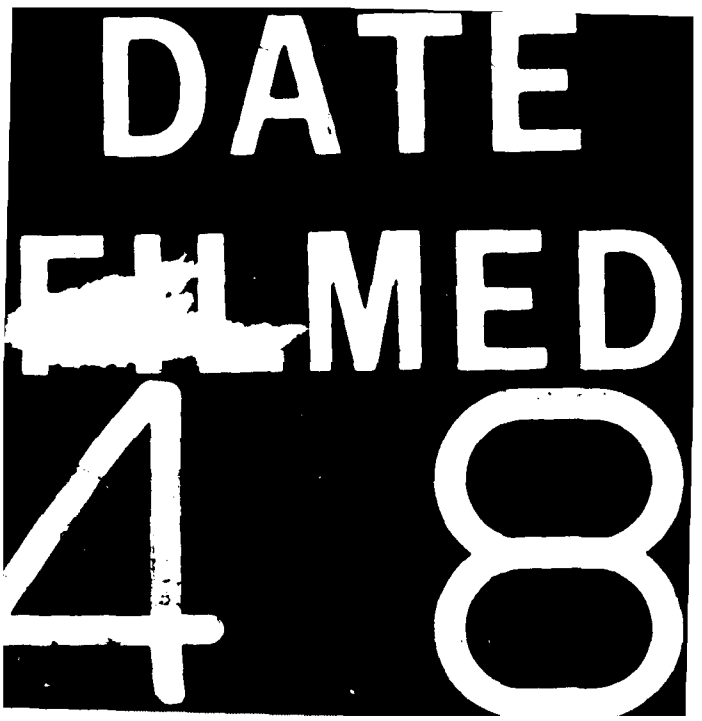
DATE
FILMED
4 8